Cell

An Endogenous Accelerator for Viral Gene Expression Confers a Fitness Advantage

Melissa W. Teng,[1,2,7] Cynthia Bolovan-Fritts,[1,7] Roy D. Dar,[1] Andrew Womack,[3] Michael L. Simpson,[4] Thomas Shenk,[3] and Leor S. Weinberger[1,2,5,6,*]

[1]The Gladstone Institutes, San Francisco, CA 94158, USA
[2]Department of Chemistry and Biochemistry, University of California San Diego, La Jolla, CA 92093, USA
[3]Department of Molecular Biology, Princeton University, Princeton, NJ 08544, USA
[4]Center for Nanophase Materials Science, Oak Ridge National Lab, Oak Ridge, TN 37831, USA
[5]Department of Biochemistry and Biophysics
[6]QB3: California Institute for Quantitative Biosciences
University of California San Francisco, CA 94158, USA
[7]These authors contributed equally to this work
*Correspondence: leor.weinberger@gladstone.ucsf.edu
http://dx.doi.org/10.1016/j.cell.2012.11.051

SUMMARY

Many signaling circuits face a fundamental tradeoff between accelerating their response speed while maintaining final levels below a cytotoxic threshold. Here, we describe a transcriptional circuitry that dynamically converts signaling inputs into faster rates without amplifying final equilibrium levels. Using time-lapse microscopy, we find that transcriptional activators accelerate human cytomegalovirus (CMV) gene expression in single cells without amplifying steady-state expression levels, and this acceleration generates a significant replication advantage. We map the accelerator to a highly self-cooperative transcriptional negative-feedback loop (Hill coefficient ~7) generated by homomultimerization of the virus's essential transactivator protein IE2 at nuclear PML bodies. Eliminating the IE2-accelerator circuit reduces transcriptional strength through mislocalization of incoming viral genomes away from PML bodies and carries a heavy fitness cost. In general, accelerators may provide a mechanism for signal-transduction circuits to respond quickly to external signals without increasing steady-state levels of potentially cytotoxic molecules.

INTRODUCTION

Biological signaling circuits, like electrical circuits, face a fundamental tradeoff between speed and amplitude (Alon, 2007; Savageau, 1976). That is, a faster rate of initial increase is typically obtained at the cost of a higher steady-state level. This tradeoff creates an evolutionary pressure when quick turn-on of a signaling molecule is essential, but the signaling molecule is cytotoxic at high levels, as with inflammatory cytokines (Cauwels and Brouckaert, 2007), many viral systems (Dwarakanath et al., 2001), and even the fever response (Roth et al., 2006). For example, herpes viruses must quickly express viral genes that modulate the host-cell environment into a replication-favorable state, but these genes often yield cytotoxic products when expressed at high levels and can prematurely damage the cell before an optimal number of viral progeny are produced. Here, we investigate mechanisms that may optimize this "rate-versus-level" tradeoff to generate a functional advantage.

We utilize the human herpes virus cytomegalovirus (CMV) because many of the viral processes that alter the host-cell environment have been well characterized (Mocarski et al., 2006). CMV infects a majority of the world's population and is a leading cause of birth defects and a leading cause of morbidity and mortality in the immunocompromised population. The virus initiates an infectious program within the cell by expressing its 86 kDa viral transactivator protein Immediate-Early 2 (IE2), which is a promiscuous transactivator of viral promoters and is essential for viral replication (Stinski and Petrik, 2008) but is also highly cytotoxic (Dwarakanath et al., 2001; Sanders et al., 2008). CMV must quickly express IE2 to establish a replication-favorable environment but also limit IE2 levels to avoid prematurely compromising the cell's ability to produce viral progeny. IE2, along with IE1, is encoded by a precursor mRNA expressed from the CMV Major Immediate-Early (MIE) promoter, which directs all subsequent viral gene expression and is considered to be the chief regulator of the lytic cycle (Stinski and Petrik, 2008). The MIE promoter (MIEP) is exceptionally strong and encodes multiple transcription factor-binding sites within its ~500 nucleotide enhancer (Stinski and Isomura, 2008). The MIEP is also autorepressed by IE2 via direct DNA binding to a 12-nucleotide *cis repression sequence* (*crs*) located between positions −13 and +1 relative to the transcriptional start site (Macias and Stinski, 1993). The impact of IE2 autoregulation upon the virus life cycle is largely unknown.

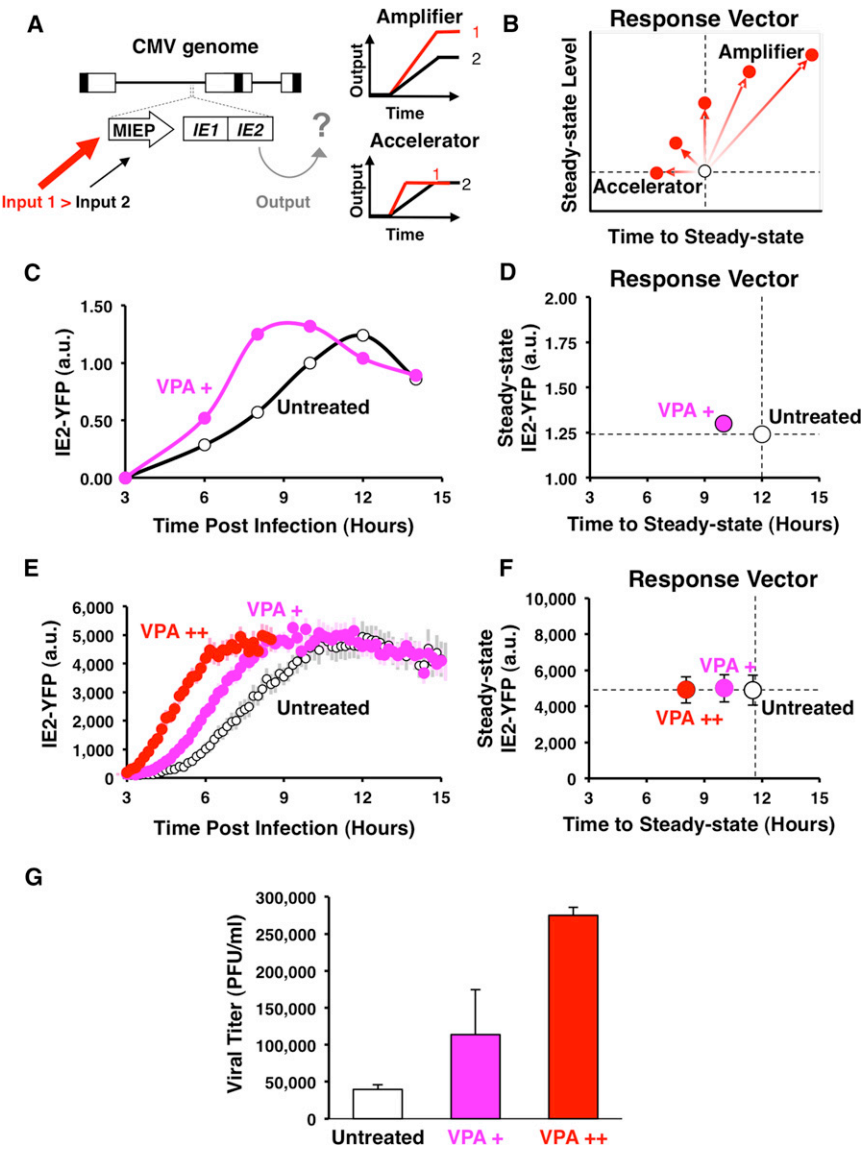

Figure 1. CMV Encodes an Endogenous Accelerator of Gene Expression and Acceleration Provides a Viral Replication Advantage

(A) Schematic of the CMV genome (~230 kb) with the MIE regulatory circuit (~5 kb) expanded. Increased inputs (transcriptional activation) to the MIE promoter could result in either increased output of protein levels (amplifier) or acceleration of gene expression without amplification of level (accelerator).

(B) The "response-vector" allows convenient comparison between output time-lapse trajectories (i.e., white versus red points) in terms of steady-state level versus the time to steady state. Circuits that act as amplifiers respond to increased input by shifting vertically or diagonally to the upper right, whereas circuits that act as "accelerators" respond by shifting horizontally left.

(C) Quantitative western blot analysis of IE2-expression levels during CMV infection from 3 h.p.i., showing acceleration in presence of VPA (pink) but no amplification in IE2 levels compared to the untreated control (white).

(D) Response-vector map of western blot data. VPA pretreatment (pink) decreases time to steady-state without increasing steady-state IE2-YFP levels when compared to the untreated control (open circles).

(E) Single-cell time-lapse microscopy of IE2-YFP levels for an untreated infection (open circles) and infection in the presence of increasing exposure to the histone-deacetylase inhibitor VPA (72 hr VPA pretreatment in red, 24 hr VPA pretreatment in pink). Each trajectory is an average of 20 cells with ± 1 SE in lighter background color.

(F) Response-vector map of single-cell microscopy data, showing that increasing VPA pretreatment (pink, red) decreases time to steady-state without increasing steady-state IE2-YFP levels when compared to the untreated control (open circles). Error bars (gray) = ±1 SE.

(G) Acceleration produces a significant fitness advantage for the virus as measured by CMV wild-type viral titers after a single round of infection (measured by plaque forming units, PFU/ml) on the peak day of viral production (day 4) after infection at MOI = 1. Average viral titers are shown in the absence of VPA (white) and for increasing VPA exposure (red, pink); Error bars = ±1 SD. See also Figure S1 and Movies S1, S2, S3.

Using an integrated approach that couples mathematical modeling with quantitative time-lapse microscopy, we show that IE2 negative feedback is highly cooperative, which allows the virus to overcome the rate-versus-level tradeoff (Figure 1A) by accelerating IE2 gene expression without any measureable increase in the steady-state expression level. To simplify comparison of level and rate, we introduce the "response vector," which maps time-lapse trajectories into points on a two-dimensional plane in terms of time to reach steady state and level of expression. Circuits that respond upward (or upward and to the right) in response-vector space are amplifiers, whereas circuits that respond in a horizontal leftward direction, like the IE2 circuit, are accelerators (Figure 1B). Strikingly, the IE2 circuit appears to be a "pure" accelerator circuit that exhibits an almost perfectly horizontal response vector. This finding may lead to other examples where tuning the expression rate, rather than the expression level, enhances fitness.

RESULTS

Transcriptional Acceleration Without Amplification in CMV

We examined MIE gene-expression levels after increasing MIEP activity by using transcriptional activators known to upregulate MIEP activity (Choi et al., 2005; Fan et al., 2005; Hummel and Abecassis, 2002). These transcriptional activators, Valproic

Acid (VPA), Trichostatin A (TSA), or Tumor Necrosis Factor Alpha (TNF-α), appear to accelerate IE2 expression but do not amplify IE2 protein levels, as measured by quantitative western blot (Figures 1C and 1D, see also Figure S1 available online). To test whether IE2 was being accelerated (but not amplified) within single cells, quantitative live time-lapse microscopy was used to track single cells undergoing infection by a recombinant CMV encoding yellow fluorescent protein (YFP) fused to the IE2 open reading frame (Movie S1). This recombinant CMV IE2-YFP virus replicates with wild-type kinetics and IE2-YFP levels are equivalent to wild-type IE2 levels (Figure S1). In agreement with previously reported IE2 fusion viruses, the IE2-YFP fusion protein correctly localizes to ND10 domains during infection (Sourvinos et al., 2007). Strikingly, increasing the activity of the MIEP by VPA pretreatment significantly accelerates IE2 expression in single cells but does not amplify steady-state IE2 levels in these single cells (Figures 1E and 1F)—a result also observed under TSA or TNF-α treatment (Figure S1). Flow cytometry analysis (Figure S1), confirms that acceleration without amplification is not an artifact of image processing.

To rule out the possibility that these results were caused by changes in cell physiology induced by pretreatment with VPA (or TSA or TNF-α), we also generated an IE2-YFP virus that carried increased levels of the viral transactivator pp71 (Bresnahan and Shenk, 2000) and confirmed that this pp71+ virus, with high levels of packaged pp71 tegument factor, accelerates IE2 expression in the absence of pretreatment (Figure S1). As an additional control, a generalized transcriptional activator that does not specifically activate the MIE promoter during active infection was used, and it fails to accelerate IE2 expression in single cells (Figure S1). These controls argue that accelerated rates of MIE expression result specifically from increased activation of the MIE promoter and not from generalized activation of the target cell. Thus, the MIE circuit appears to act as an "accelerator" that allows only the rate of IE2 expression to change without allowing significant change in the steady-state levels of IE2.

Acceleration Provides a Fitness Advantage for the Virus

Previous studies in RNA viruses have noted that small increases in a single round of replication are sufficient to allow a viral strain to competitively exclude other "less fit" strains in resource-limited environments; in other words, the strain with the highest basic reproductive number (R_0), which is measured during a single round of infection, wins and excludes all other competing strains, even if that strain's R_0 is only marginally greater than the closest competitor (Nowak and May, 2000).

To test whether acceleration of IE2 expression provides any functional advantage for the virus, we analyzed viral replication kinetics after the first round of viral maturation (~96 hr) from cells infected with CMV IE2-YFP virus (Figure 1G). The results show that incremental increases in transcriptional activation, and the resulting acceleration in MIE kinetics, generate correlated increases in viral replication fitness with a 72 hr VPA pretreatment, yielding an approximately 5-fold increase in viral replication compared to the untreated control. IE2 acceleration and enhanced replication are also observed in the low-passage clinical CMV isolate TB40-E, which exhibits a 9-fold increase in titer (Figure S1).

Acceleration Without Amplification Requires Highly Self-Cooperative Negative Feedback, and IE2 Exhibits a Hill Coefficient, *H*, of *H*~7

Next, we set out to identify the mechanisms driving acceleration in the CMV MIE circuit. Based on previous studies showing that negative feedback speeds a circuit's "response time," (i.e., the time required for a circuit to approach to its respective steady-state level) (Black, 1999; Gardner et al., 2000; Kobayashi et al., 2004; Rosenfeld et al., 2002; Savageau, 1976), we hypothesized that acceleration without amplification would likely utilize negative feedback. By employing a rate-balance analysis, we find that negative feedback encoding a high "Hill" coefficient *(H)* is theoretically sufficient to generate acceleration without amplification (Figure 2A), whereas alternate simple models cannot generate acceleration without amplification (Supplemental Information, Figure S2), in agreement with previous studies (Black, 1999; Rosenfeld et al., 2002; Savageau, 1976). Based on this analysis, we constructed a nonlinear ordinary differential equation (ODE) model of the CMV MIE circuit (Supplemental Information, Figure S2, Table S1) and performed nonlinear least-squares regression of the model by using the single-cell microscopy data to estimate the *H* value of the IE2 negative feedback. *H*~7 generates the best fit to the single-cell time-lapse microscopy data (Figure 2B), and sensitivity analysis demonstrates that $H < 6$ and $H > 8$ cannot generate good fits to the data even when all other parameters are allowed to vary across all physiological parameter space (Figure S2). These simulation results demonstrate that a negative-feedback model with a high *H* is sufficient to generate acceleration without amplification and predict that the IE2 circuit requires negative feedback with $H \gg 1$ to function as an accelerator.

H is traditionally measured by dose-response approaches, which are "open loop" (i.e., feedback is removed from the system). However, for transactivators that are cytotoxic at high doses, such as IE2, the dose-response method destroys the cell before the response can be measured (data not shown). To circumvent this cytotoxicity problem, we developed a "closed loop" single-cell analysis method to analyze how a circuit's output (steady-state protein levels) saturates as a function of increasing promoter activation and varying *H* values (Figure 2C). This method essentially measures the change in steady-state levels as a function of increasing promoter strength.

To measure *H* via this closed-loop method, flow-cytometry measurements of steady-state GFP levels were collected for a minimal negative-feedback circuit encoding the full-length MIEP driving IE2 and GFP (MIEP-IE2-IRES-GFP) and compared to a minimal nonfeedback circuit encoding the full-length MIEP driving GFP (MIEP-mCherry-IRES-GFP), which acts as the nonfeedback control circuit. By increasing the MIEP activity with transcriptional activators (e.g., TSA or VPA) the response of each circuit can be measured (Figure 2C), and these responses can then be compared to theoretically predicted responses for varying *H* levels (Figure 2C). As expected for the nonfeedback circuit, a linear increase in activator results in a linear increase in GFP steady-state levels (black). However, for the MIEP-IE2-IRES-GFP negative-feedback circuit (red), the equivalent linear

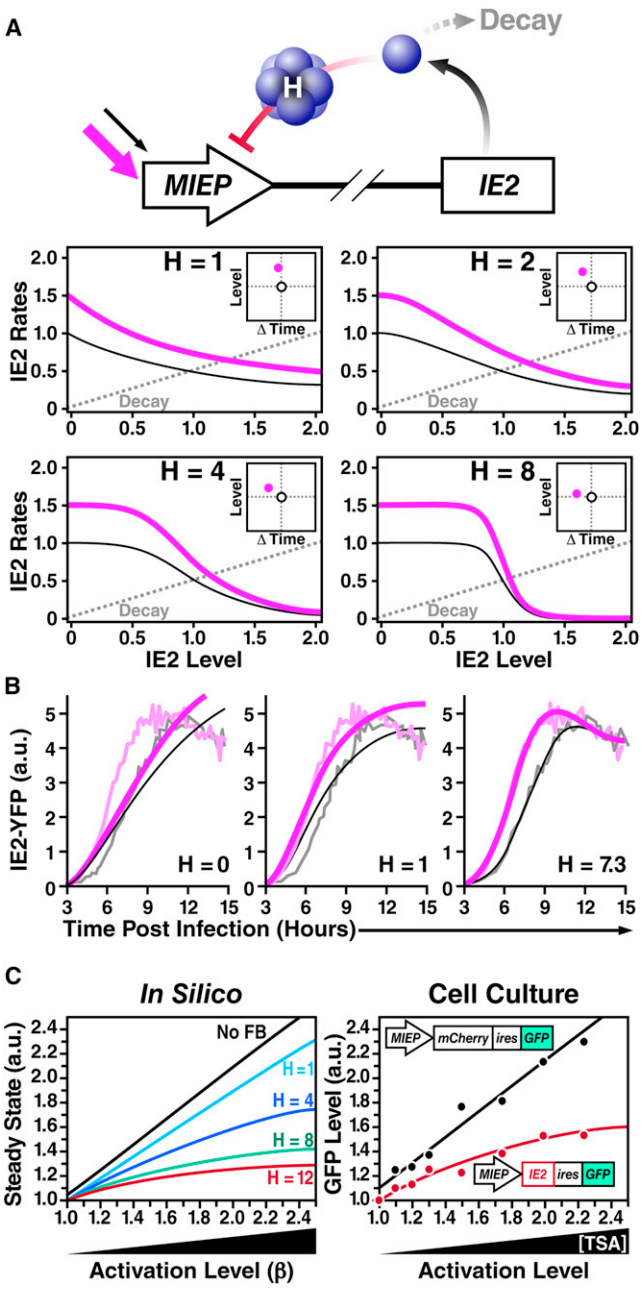

Figure 2. Highly Self-Cooperative Negative Feedback Is Needed to Generate an Accelerator Circuit and IE2 Encodes Negative Feedback with a High Hill Coefficient, *H*∼7

(A) Schematic and rate-balance analysis of a simplified negative-feedback model: $dx/dt = (\beta/(k^H + x^H)) - \delta \cdot x$ for different values of the Hill coefficient (*H*). The dashed gray line represents the decay rate, whereas solid lines (black and pink) represent synthesis rates for increasing values of β (1.0 and 1.5, respectively), which accounts for induction by a transcriptional activator that increases basal promoter activity by 1.5-fold. The points at which solid and dashed lines meet represent the steady states, and the distance separating the solid and dashed lines represents the rates of expression. Rate-balance analysis is shown for four values of *H*. High values of *H* allow the expression rate to increase without amplification in the steady-state level. Insets: response vectors showing the change in steady-state level and the change in time to steady state for each *H* value.

increase in activator input results in a significant saturation in GFP steady state. This saturation in the GFP steady-state values is consistent with the regression analysis, indicating $H \sim 7$ for IE2 negative feedback. These results indicate that IE2 negative feedback acts early during CMV infection (i.e., during the first 12 hr), which has not been reported. Taken together, the results demonstrate that the IE2 circuit encodes a highly self-cooperative negative feedback with an *H* value sufficient to generate an accelerator that effectively abolishes IE2 amplification under different inputs.

Highly Self-Cooperative IE2 Feedback Results from IE2 Homo-Multimerization

We suspected that the high *H* value might be due to IE2 homo-multimerization, based on (1) in vitro biochemical studies reporting that IE2 peptide fragments can homomultimerize when binding to DNA (Chiou et al., 1993; Waheed et al., 1998), and (2) well-characterized mechanisms in other negative-regulation circuits encoding $H > 1$ (Chen et al., 1994; Hooshangi et al., 2005). To assay for IE2 homomultimerization in real time during CMV infection, we utilized polarization anisotropy Förster Resonance Energy Transfer (FRET) imaging, which can differentiate between monomers and higher-order homomultimers (Gautier et al., 2001). During the first 16 hr of infection, IE2-YFP exhibits a strong homo-FRET anisotropy (*r*) signal corresponding to high-order IE2 homomultimerization (Figure 3A).

We next used an established theoretical model (Runnels and Scarlata, 1995) to estimate the number of individual IE2 monomers that might be interacting within an IE2 homomultimer to generate the measured polarization anisotropy signal. Although the model cannot precisely calculate the number of monomers making up the homomultimer—because the distance between individual IE2 monomers is not known—a lower limit on the number of IE2 monomers within the homomultimer can be estimated with confidence, under the most conservative assumption that the distance between each IE2-YFP monomer is the diameter of the YFP molecule (24 Å). Under this maximally conservative assumption, the measured anisotropy shift $(r \geq 0.5 \rightarrow r \approx 0.1)$ is consistent with an IE2 homomultimer composed of at least five to six IE2 monomers (Figure 3B).

(B) Nonlinear least-squares regression of single-cell time-lapse microscopy data from Figure 1E to a mathematical model of the CMV MIE circuit (Supplemental Information) showing the best-fit curve of $H = 7.3$ (right). Gray data points are untreated trajectories from Figure 1D, whereas pink data points are VPA+ trajectories from Figure 1D. Poor data fits are generated when *H* is fixed at $H = 1$ or $H = 0$ (no feedback) despite letting all other free parameters in the model vary (middle and left, respectively); sensitivity analysis shows that setting $H < 6$ or $H > 8$ generates poor fits to the data (Figure S2).

(C) Closed-loop dose-response analysis to measure *H* for the IE2 circuit. Left: steady-state solutions for the minimal negative-feedback ODE model (from A) as a function of increasing basal promoter strength β for different *H* values. Right: live-cell flow cytometry measurements of a non-feedback CMV MIEP-mCherry-IRES-GFP control circuit (black) and a minimal negative-feedback CMV MIEP-IE2-IRES-GFP circuit (red) induced to different levels of activation by TSA treatment. CMV MIEP-mCherry-IRES-GFP shows a linear increase in final level, whereas CMV MIEP-IE2-IRES-GFP shows saturation in steady-state level consistent with $H \sim 7$. See also Figure S2, Table S1, and Movie S4.

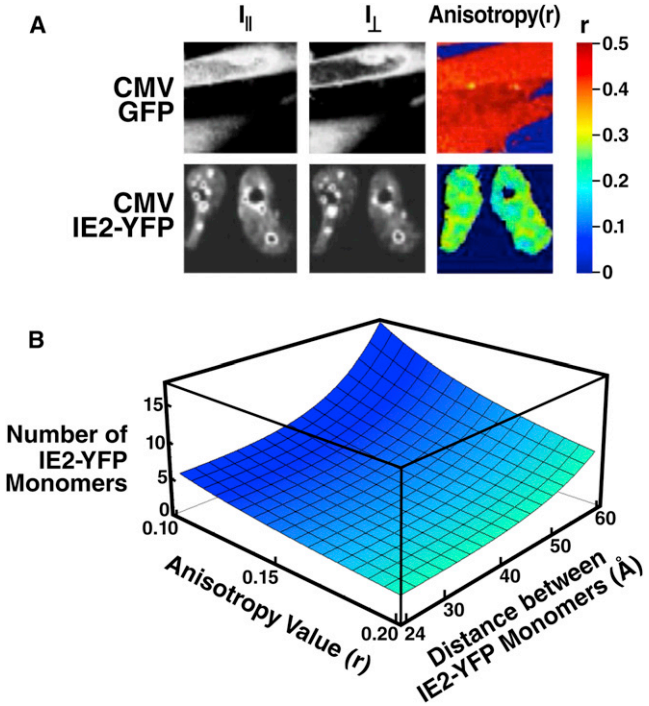

Figure 3. IE2 Forms a High-Order Homo-Multimer that Can Account for a High *H* Value

(A) Direct measurement of IE2 homomultimerization by two-photon steady-state homo-FRET in live cells during CMV infection. CMV IE2-YFP-infected cells were imaged to determine fluorescence polarization anisotropy (*r*) at 15 hr postinfection and compared to cells infected with a control CMV GFP virus. An $r \approx 0.5$ represents no FRET exchange and is the two-photon theoretical maximum anisotropy for a GFP or YFP monomer. IE2-YFP exhibits significant depolarization and homo-FRET exchange in the nucleus and especially at subnuclear foci, indicating the presence of a high-order IE2 homomultimer.

(B) Calculation of a lower limit for the number of IE2 monomers present in the IE2 multimer, based on measured anisotropy values. Plotted surface is the solution to the theoretical formula that accounts for the number of IE2-YFP monomers (*N*) in a complex participating in FRET exchange that could account for a given value of *r* based on the distance between each monomer (*R*). The formula estimates a lower limit for YFP monomers in a homomultimer that could generate a given *r*. Under the maximally-conservative assumption that all YFP monomers are as tightly packed as physically possible (R = 24 Å), the minimum number of IE2-YFP monomers participating in homo-FRET exchange that could generate an anisotropy value of $r = 0.1$ is approximately 6. See also Figure S3.

Importantly, the IE2-YFP monomers are likely separated by >24 Å, and the results of Figure 3B show that the measured anisotropy shift is well within the theoretical range of IE2 forming a homoheptamer or higher order homomultimer at the ND10 foci. Measurements of IE2 diffusion kinetics from fluorescence recovery after photobleaching (FRAP), support the assertion that IE2 aggregates at ND10 domains in infected cells (Figure S3). Despite these direct measurements of IE2 homomultimerization in live cells during active infection, structural studies would definitively establish the presence of a high-order IE2 homomultimer bound to DNA.

In summary, results from three independent measurements, namely (1) regression fitting of a minimal ODE model to single-cell CMV IE2-YFP trajectories, (2) the "closed-loop" analysis of the isolated IE2 feedback circuit, and (3) homo-FRET imaging of IE2-YFP, all point toward the IE2 negative-feedback circuit as operating with a high Hill coefficient ($H \sim 7$). These data argue that IE2 homomultimerization is a core factor in establishing the high Hill coefficient of this transcriptional negative-feedback circuit, and that homomultimerization underlies the circuit's ability to act as an accelerator.

A Minimal-Accelerator Circuit Provides a Fitness Advantage outside the Infection Setting

To verify that highly self-cooperative negative feedback is sufficient to generate an accelerator, we reconstructed a minimal IE2 feedback circuit lacking all other viral elements and analyzed it completely outside the virus infection setting. The minimal IE2 feedback circuit was constructed using a lentiviral vector expressing only IE2 and GFP from either the full-length wild-type MIEP or a mutant version of the MIEP in which three nucleotides in the *crs*-binding site are mutated to eliminate IE2 binding (Macias and Stinski, 1993) (Figure 4A). Both wild-type and mutant *Δcrs* lentiviral circuits were stably integrated into the cellular genome. The minimal wild-type circuit stably expresses IE2 (Figure S4), and two-color imaging confirms that the MIEP exhibits comparable kinetics both within the context of the virus and stably integrated in host-genome DNA (Figure S4). As predicted from the model, the minimal mutant circuit exhibits substantially increased mean GFP fluorescence intensity (Figures 4B and S4). The minimal mutant circuit fails to generate acceleration, instead acting as an amplifier (Figure 4C), whereas the wild-type feedback circuit generates acceleration (Figure S4), even in the absence of all other viral elements. Cells carrying the wild-type accelerator circuit also exhibit a profound viability advantage over cells carrying mutant amplifier circuit (Figure 4D). Dramatically, cell populations carrying the minimal wild-type accelerator circuit maintain IE2 and GFP expression, whereas cell populations carrying the minimal mutant circuit exhibit a rapid loss of IE2 and GFP expression that increases over time (Figures 4E and S4). Genomic PCR (Figure 4F) confirms that loss of IE2 and GFP expression is due to a loss of cells carrying the stably integrated mutant circuit, not from silencing of the integrated MIEP. These data argue that cells carrying the mutant circuit express higher IE2 levels and undergo increased cell death, leading to these cells being outcompeted from the population. Thus, a minimal IE2 accelerator circuit provides cells with a dramatic fitness advantage over a comparable IE2 amplifier circuit, even in the absence of all other viral factors.

Converting the Accelerator to an Amplifier Generates a Severe Fitness Cost for the Virus

To determine whether negative feedback is necessary for the MIE circuit to act as an accelerator in the context of the virus, we constructed a *Δcrs* virus by bacterial artificial chromosome (BAC) mutagenesis of the three nucleotides in the *crs*-binding site (Figure 5A). In agreement with modeling predictions and the minimal circuit observations (Figure 4), this *Δcrs* mutant virus acts as an amplifier generating a ~1.5-fold amplification in single-cell expression levels in the presence of MIEP activators

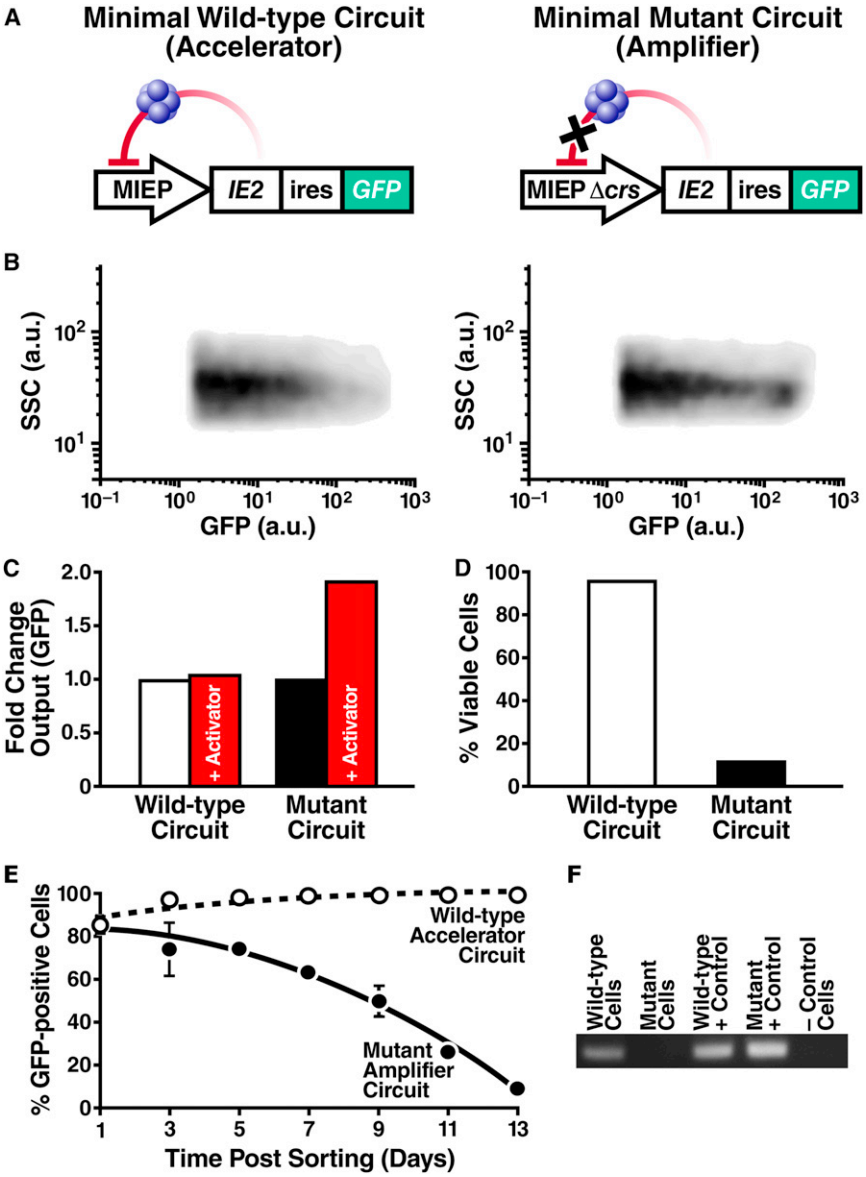

Figure 4. A Minimal IE2 Accelerator Circuit Provides a Fitness Advantage Outside the Context of Viral Infection

(A) Schematics of the minimal wild-type accelerator circuit MIEP-IE2-IRES-GFP (left) and minimal mutant amplifier circuit MIEP*Δcrs*-IE2-IRES-GFP (right). Both circuits are lentiviral vectors and encode an IRES element between IE2 and GFP.

(B) Flow cytometry density plot of cells stably expressing the wild-type accelerator (left) or the mutant amplifier (right) circuit that exhibits ~8-fold higher mean GFP.

(C) Fold increase in GFP for the wild-type accelerator and mutant amplifier circuits in the absence (white, black) or presence (red) of TSA.

(D) Percentage of live cells (by flow cytometry) after 14 days of TSA treatment. TSA treatment has little effect on viability of cells expressing the wild-type accelerator circuit (white) but leads to significantly decreased viability in cells expressing the mutant amplifier cells (black).

(E) Flow cytometry time-course of the % of GFP expressing cells for the accelerator (white) and amplifier (black) circuits. GFP expression is lost from the cells transduced with the mutant amplifier circuit but is maintained in cells transduced with wild-type accelerator circuit (averages of three replicates shown in bold with ±1 SD).

(F) PCR amplification of the MIEP locus from: cellular genomic DNA of cells transduced with either wild-type accelerator circuit or mutant amplifier circuit on day 14 (lanes 1 and 2); plasmid DNA of wild-type accelerator or mutant amplifier lentiviral vector (lanes 3 and 4, positive PCR controls); naive nontransduced cells, negative control (lane 5). At day 14, the mutant amplifier circuit has been lost from the genomic DNA of the transduced population but the wild-type accelerator circuit remains present in the genomic DNA of the transduced population. See also Figure S4.

(Figures 5B and S5) and exhibits virtually no acceleration (Figure 5C).

Strikingly, replication of this mutant amplifier virus is severely compromised in the presence of activators (Figures 5D and S5). These data agree with the minimal-circuit data that amplification of IE2 levels is deleterious for the cell, leading to decreased viral output. Potential toxicity of VPA or TSA exposure alone cannot account for reduced viral replication because neither activator reduces replication fitness of the parent virus (Figure S5).

To rule out secondary mutations outside the *crs* region that could be responsible for amplification, these results were verified in two independently isolated BAC clones and sequencing 1 kb upstream and downstream of the *crs* verified the absence of secondary mutations (data not shown). The generation of a "rescue" virus with wild-type IE2-expression kinetics (described below and in Figure 7) independently verifies that secondary mutations do not account for the amplifier phenotype or reduced fitness. This absence of secondary mutations is not unexpected given the reported stability and specificity of BAC mutagenesis for CMV (Reddehase and Lemmermann, 2006).

The Loss of the Accelerator Circuit in the *Δcrs* Amplifier Mutant Is Buffered by Reduced MIEP Activity through Mislocalization of Incoming Viral Genomes

Although theory predicts that removal of negative feedback should increase IE2 steady-state levels (as in the minimal circuit), the biology of IE2 cytotoxicity and the presence of the accelerator circuit in the wild-type virus suggest that over the course of viral evolution, there is strong selection for mechanisms to maintain low IE2 levels. Therefore, to determine how the *Δcrs* amplifier mutant virus can maintain any viability even in the absence of activators (Figure 5D), we tested whether IE2

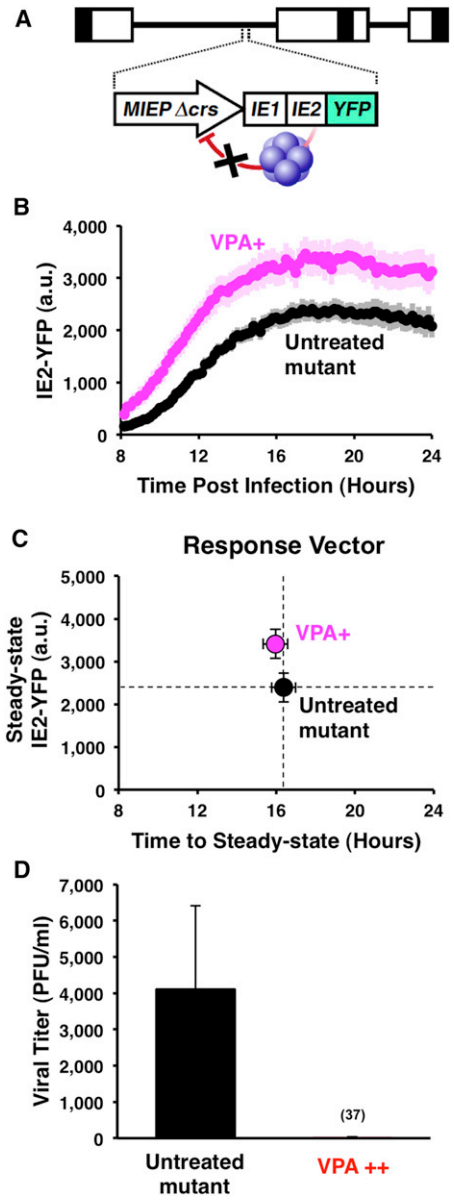

Figure 5. Converting the IE2 Accelerator to an Amplifier—by Eliminating Negative Feedback—Generates a Severe Fitness Cost for the Virus

(A) Schematic of the mutant CMV Δ*crs* mutant virus.

(B) Single-cell time-lapse microscopy of cells undergoing infection with CMV Δ*crs* mutant in presence of 24 hr pretreatment of VPA (pink) or absence of VPA (black). Trajectories are averages of 20 cells (bold) together with ±1 SE (lighter background). The CMV *Δcrs* mutant displays an ~1.5-fold amplification in IE2 levels in single cells in response to VPA.

(C) Response-vector map of single-cell microscopy data showing that the *Δcrs* mutant virus amplifies steady-state IE2-YFP levels compared to the untreated control (black). Error bars (gray) = ±1 SE.

(D) Replicative fitness of the CMV *Δcrs* mutant in presence (red) and absence (black) of a 72 hr VPA treatment as measured by PFU/ml on the peak day of viral production (day 10) after infection at MOI = 1. Average values are shown with ±1 SD. Decreased replication is not due to drug toxicity on the infected cells (see Figure S5).

untreated steady-state levels are increased, similar to the minimal circuit setting, or whether the mutant virus employs compensatory mechanisms to keep IE2 levels low. Single-cell imaging and flow cytometry analysis reveal that IE2 steady-state levels in the *Δcrs* mutant amplifier virus (in the absence of activators) are essentially the same as IE2 levels in the wild-type virus (Figures 6A and S6) but the rate of IE2 expression is significantly slower in the mutant (Figure 6B). Based on literature indicating that subnuclear PML bodies facilitate transcription from the MIEP (Sourvinos et al., 2007), we tested whether reduced IE2 levels were the result of decreased MIEP activity due to *Δcrs* mutation-induced mislocalization of incoming viral genomes away from PML bodies. Although the wild-type virus exhibits IE2 localization to PML bodies, the *Δcrs* mutant virus displays virtually no IE2-positive foci during early infection (Figure S3), and immunofluorescence analysis shows that *Δcrs* mutant viral genomes do not colocalize with PML bodies (Figure 6C). To confirm that PML-body mislocalization reduces IE2 levels, we infected a cell line lacking PML bodies (Everett and Chelbi-Alix, 2007) and observed significantly reduced steady-state IE2 levels (Figure 6D). In summary, the *Δcrs* mutant amplifier virus appears to compensate for the lack of accelerator circuitry by reducing MIEP transcriptional strength, through misdirecting incoming viral genomes away from sub-nuclear PML bodies.

The minimal circuit is integrated into the genome as a single-copy lentiviral provirus and MIEP does not appear to be influenced by PML body localization in this context.

Reduced MIEP Activity Decelerates IE2 Expression and Carries a Heavy Fitness Cost

Because the amplifier mutant and wild-type accelerator viruses exhibit equivalent IE2 steady-state levels but different rates of IE2 expression, we next tested whether the mutant's reduced fitness could be rescued by acceleration. To do this, we provided the mutant virus with the opportunity to regain accelerator circuitry through homologous recombination, by cotransfecting cells with the full *Δcrs* mutant virus genome together with a short 1 kb DNA fragment of the MIEP encoding the wild-type *crs* sequence. This approach to generate recombinant "rescue" virus (Figure 7A) creates a "fitness competition" because the mutant must compete with any rescue that arises within the culture. After culturing the cotransfected cells for 2 weeks (the typical time for growth of CMV IE2-YFP in culture), all observable CMV-positive plaques analyzed are rescue virus that exhibit accelerated expression kinetics (Figure 7B), and fitness comparable to that of wild-type virus (Figure 7C). The fact that high-titer accelerator rescue virus can be isolated from a background *Δcrs* infection while no detectable *Δcrs* virus can be isolated from this background indicates that viruses encoding the accelerator circuit directly outcompete viruses encoding the mutant amplifier even in the absence of transcriptional activator drugs. Sequencing results confirm that in the rescue virus the *Δcrs* locus is restored to the wild-type sequence and that the rescue virus exhibits a complete recovery of the accelerator phenotype (Figure S7). These results show that a slower rate of IE2 expression is sufficient to generate a heavy fitness cost even when IE2 levels are not elevated.

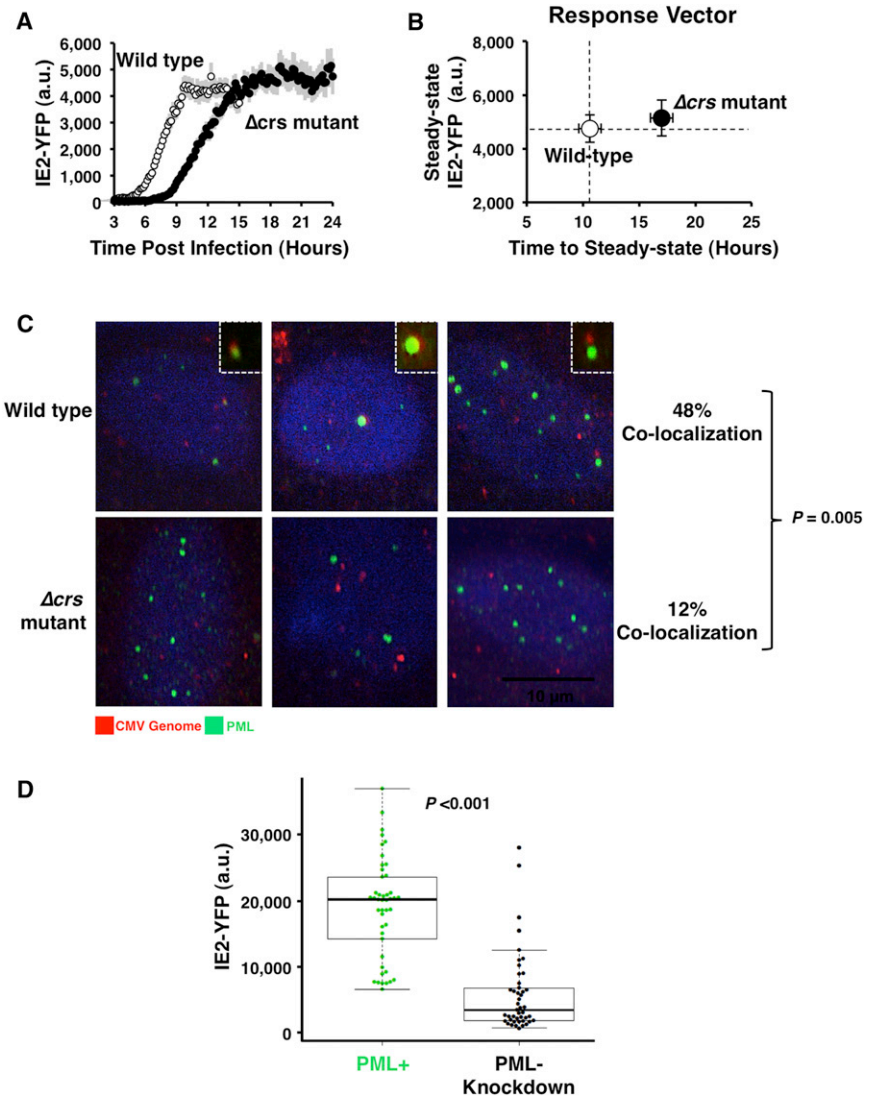

Figure 6. Mutation of the *crs* in the CMV Genome Results in Inefficient Formation of IE Transcriptional Centers and Lower IE2-YFP Expression

(A) Single-cell time-lapse microscopy analysis comparing CMV IE2-YFP virus, referred to as "wild type" (white), to *Δcrs* amplifier mutant virus (black); infections imaged in parallel on the same day under the same conditions. Error bars (gray) = ±1 SE.

(B) Response-vector map showing that the *Δcrs* amplifier mutant virus (black) exhibits decelerated IE2 kinetics but no change in IE2 steady-state level compared to wild-type (white). Error bars = ± 1 SE

(C) Immunofluorescence micrographs of cells infected with either wild-type CMV (top) or the *Δcrs* mutant virus (bottom) and stained for CMV genome (red), PML protein (green), and DNA (blue). CMV genomes and PML bodies appear to colocalize at a significantly higher frequency ($p < 0.01$) in cells infected with wild-type CMV virus compared to *Δcrs* amplifier mutant virus. Insets: representative colocalization of CMV genomes and PML bodies.

(D) Steady-state IE2-YFP levels from single-cell microscopy in conventional PML+ cells (green) cells or PML- knockdown cells (black). Both cell types were infected with "wild-type" CMV IE2-YFP virus. Bold black lines in the box plot are the median IE2-YFP levels, boxes represent lower and upper quartile, and whiskers represent 1.5 interquartile range (IQR) of the lower and upper quartiles. PML knockdown significantly reduces IE2-YFP levels ($p < 0.001$). See also Figure S6.

DISCUSSION

This study characterizes an endogenous accelerator circuit, and shows that acceleration of transcriptional response time, without modulation of steady-state levels, can confer a fitness advantage. The fitness advantage is unlikely to result solely from faster IE2 expression but rather from IE2 driving acceleration of downstream viral expression, because viral *cyto*pathic *e*ffect (CPE) is observed earlier when IE2 kinetics are accelerated (Movies S2 and S3), and other key steps in the viral life cycle are decelerated in *Δcrs* viruses (Isomura et al., 2008). Conversely, it is unlikely that the fitness advantage results from non-IE2-driven alternate pathways because the same transcriptional activators that generate acceleration in the wild-type virus generate amplification with severe fitness loss in the *Δcrs* mutant amplifier virus and in minimal synthetic circuits where only the accelerator has been removed. The alternate pathway hypothesis is also difficult to reconcile with our finding that MIEP activators (pp71, VPA, TSA, and TNF-α) generate acceleration, whereas broad-spectrum non-MIEP activators (5Aza-C) cannot generate acceleration (Figure S1). The finding that a rescue virus (which only differs in rate of IE2 expression not level) outcompetes the *Δcrs* amplifier mutant, further argues that the expression rate drives the fitness advantage. These findings demonstrate a functional role for IE2 negative feedback in maintaining viral fitness.

The unique architecture of IE2 negative feedback and the circuit's ability to act as an accelerator lies in the high Hill coefficient, $H \sim 7$, which to our knowledge is the highest value yet recorded for a transcriptional autoregulatory circuit. Although a number of mechanisms can generate high *H* values, including multiple binding sites for an autoregulatory protein on the target DNA (Ozbudak et al., 2004) or sequential covalent modifications of an autoregulator (Deshaies and Ferrell, 2001), in the case of IE2 the *H* value may be explained by formation of a homomultimer, consisting of six to eight IE2 protein monomers that form at or around the 12 bp *crs* DNA-binding site for IE2. The formation of such a large homomultimer leads to the question of how a 12 bp sequence of DNA (just over 40 Å in length) might have the steric space requirements to support binding of this homomultimer complex, which is likely over half a megadalton with

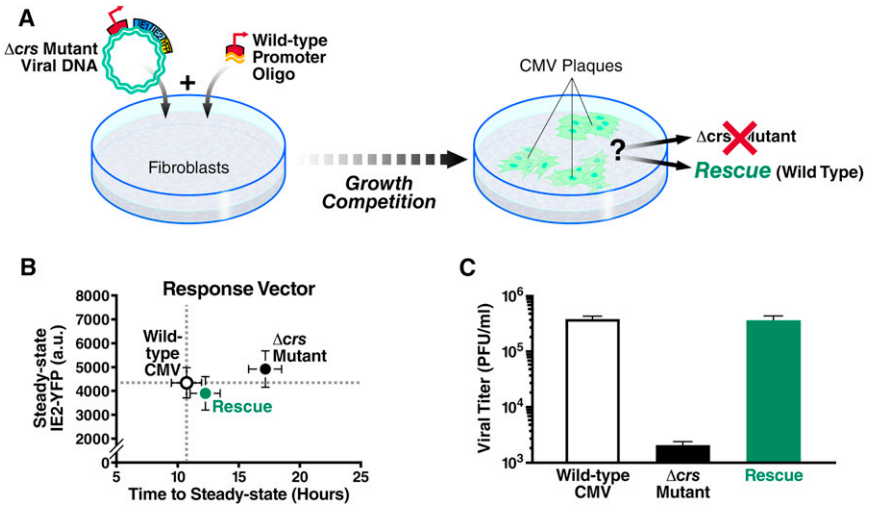

Figure 7. Loss of IE2 Acceleration, Despite Equivalent IE2 Levels, Carries a Heavy Fitness Cost

(A) Schematic of "rescue" experiment that represents a growth competition between the *Δcrs* amplifier mutant virus and "wild-type" CMV IE2-YFP.

(B) Response-vector map of single-cell microscopy showing that the rescue virus (green) generated from the mutant amplifier virus (black), has regained the accelerated expression kinetics of the wild-type virus (white) and all viruses exhibit equivalent IE2-YFP steady-state levels; all viruses (wild-type, mutant, and rescue) were imaged in parallel on the same day under the same conditions. Error bars (gray) = ±1 SE.

(C) Viral replication titers for the rescue virus (green) compared to *Δcrs* amplifier mutant (black) and wild-type viruses (white) as measured by PFU/ml on the peak day of viral production in a multistep assay (MOI = 0.1). Despite all viruses exhibiting equivalent IE2-YFP steady-state levels, the rescue virus, which has reacquired the wild-type accelerator, replicates with the same high efficiency as wild-type virus, whereas the *Δcrs* amplifier mutant virus exhibits a severe fitness disadvantage. Averages are shown in bold gray with ±1 SD. See also Figure S7.

a diameter >120 Å, approximately three times as large as the DNA-binding site itself. Notably, the eukaryotic transcription factor Sp1 binds a 10 bp DNA sequence as a homotetramer (Haase, 2010), and many viral proteins cooperatively homomultimerize to bind short palindromic DNA sequences, including the Rep 78/68 protein in adeno-associated virus, the SV40 large T antigen, and bovine papillomavirus type 1 E1 protein—all of which form homohexamers on short palindromic DNA sequences (Flint and American Society for Microbiology, 2009). Thus, homomultimer formation appears to be a property shared among diverse proteins involved in viral replication as a way to bind short, palindromic DNA sequences. The high cooperativity of IE2 regulation may also be influenced by "conditional cooperativity" (Garcia-Pino et al., 2010) because other host and viral factors, such as viral UL84, functionally interact with IE2 during the viral lifecycle (Gebert et al., 1997) and numerous covalent modifications of IE2 are reported to influence functionality (Barrasa et al., 2005; Hofmann et al., 2000). In general, highly self-cooperative negative feedback may provide a generic mechanism to optimize the rate-versus-level tradeoff.

The Mechanics of the Accelerator Circuit in Relation to Other Negative Autoregulatory Circuits

Negative feedback has long been known to speed a circuit's response time (Black, 1999; Rosenfeld et al., 2002; Savageau, 1976), which is the time required for a circuit to reach its steady-state level or some fixed percentage of its steady-state level (e.g., 50%). Compared to nonfeedback circuits, circuits encoding negative feedback (i.e., autoregulation) approach a lower steady-state level but attain this relative steady-state level faster. However, a long-running biological counterargument has been that transcriptional circuits must cross an absolute threshold (e.g., 10 molecules) and negative feedback necessarily slows (not speeds) this crossing. This incongruity, in which negative feedback speeds response time but slows threshold crossing, has led to a controversy regarding the kinetic role of negative feedback.

It has been argued that response time (i.e., 50% of some relative steady-state level) is a misleading measure and that negative feedback has no functional role in accelerating responses. The accelerator circuitry characterized here addresses this controversy because it acts as a hybrid between nonfeedback and feedback circuits. Rate-balance analysis (Figure 2A and Movie S4) shows that as the self-cooperativity is increased, the accelerator circuit behaves more and more like a nonfeedback circuit at low IE2 concentrations, allowing for faster crossing of an absolute molecular threshold. As IE2 levels approach the concentration threshold where self-cooperative negative feedback becomes active, feedback turns on very quickly (and at almost maximum strength) and sharply autorepresses the MIEP to keep the steady-state level from changing under different inputs. In the framework of electrical-circuit theory, the accelerator inverts the typical input/output transfer function and dynamically redistributes the "gain-bandwidth' relationship (see Supplemental Information). It is possible that diverse signaling pathways that employ negative feedback utilize this inversion of input/output as a means of signal discrimination or as a mechanism to approximate "perfect adaptation" (Ma et al., 2009; Muzzey et al., 2009) in steady-state levels. The high cooperativity in negative feedback may also function to suppress stochastic fluctuations (i.e., noise) that influence the behavior of decision-making circuits (Cağatay et al., 2009).

Potential Roles for the Accelerator Circuit in the Evolution of Virulence

Why might CMV have evolved the accelerator architecture over other potential mechanisms to maintain low levels of IE2? CMV's lifecycle in vivo involves replication in diverse cell types and host conditions, and the strong, easily activated MIEP is well suited to activate under these diverse conditions. The MIEP's strength is

due to numerous enhancer-binding sites that have the potential to generate large amplifications of input signal through combinatorial binding (Carey et al., 2009). Consequently, CMV's accelerator circuit may have evolved as a natural consequence of the strong MIEP to counteract and limit the inevitable amplification of signal from MIEP. An alternate mechanism would be to enhance the basal-expression strength of the MIEP, while simultaneously increasing the decay (i.e., turnover) rate of IE2. This strategy would be difficult to achieve for CMV because the MIEP is one of the strongest known promoters and the IE2 half-life is ~2.5 hr (Figure S6). Given this short half-life of IE2, coupled with the already exceptional strength of the MIEP, it may not be possible to further reduce IE2 half-life (while maintaining its essential functions) or increase the unstimulated MIEP activity level. However, this strategy may have been an evolutionary precursor to the accelerator circuit.

In settings where host responses lead to high viral loss, faster expression, and increased viral output in response to inflammatory or innate-defense factors may enable the virus to outpace host defenses. Thus, tuning of the expression rate may have evolved as a viral countermeasure to outpace the host cell's innate immune defenses. Because these considerations are not unique to CMV infection, accelerator circuitry may be a widespread architecture among gene-regulatory circuits.

EXPERIMENTAL PROCEDURES

Cloning of Recombinant Viruses

The CMV IE2-YFP virus was constructed by inserting EYFP (Clontech) to the 3′ end of IE2 exon 5 in the parent AD169 as described (Moorman et al., 2008; Yu et al., 2002).

The CMV GFP control virus (Yu et al., 2003) encodes an SV40 promoter-EGFP cassette. The CMV *Δcrs* IE2-YFP virus was constructed from the CMV IE2-YFP background as described (Cuevas-Bennett and Shenk, 2008). Viral stocks were titered by $TCID_{50}$ (Nevels et al., 2004). To verify the integrity of the CMV *Δcrs* IE2-YFP virus, a rescue virus, CMV *ΔcrsREVERT* IE2-YFP, was constructed by homologous recombination, whereby CMV *Δcrs* IE2-YFP BAC DNA (20 μg) and a ~2.5 kb wild-type MIEP DNA fragment (2.5 μg) were cotransfected by electroporation into 10^6 MRC5 cells and subjected to two rounds of plaque purification.

Cell-Culture Conditions and Drug Perturbations

MRC5 fibroblasts and life-extended human foreskin fibroblasts (HFFs) (Bresnahan and Shenk, 2000) were maintained in Dulbecco's Modified Eagle's Medium (DMEM) supplemented with 10% fetal bovine serum (FBS) and 50 U/ml penicillin-streptomycin at 37°C and 5% CO_2 in a humidified incubator. ARPE-19 cells were maintained in a 1:1 mixture of DMEM/F-12 (Mediatech) with 10% FBS (HyClone) and 50 U/ml Penicillin-Streptomycin (Mediatech). Cells were pretreated in a final concentration of 1 mM VPA (Calbiochem).

Quantitative Western Blot Analysis

MRC5s at ~60% confluency were infected at MOI = 1. To synchronize viral entry, adsorption was done at 4°C for 30 min, cells were washed once in PBS (Mediatech), fresh medium was added, and cells placed in a 37°C in a humidified CO_2 incubator. Time points were collected every 1–2 hr for 20–24 hr as indicated. Sample collection, protein transfer, and blot preparation were as described (Bolovan-Fritts et al., 2004), and samples were loaded and separated on precast SDS PAGE 10% or 7.5% bisacrylamide gels (BioRad).

For quantitative IE2 detection, the 1° antibody MAB810 (Millipore) was used at 1:100 and 2° antibody 926-32212 (LI-COR) was used at a dilution of 1:20,000. For normalization, anti-beta tubulin antibody 26-42211 (LI-COR) used at a dilution of 1:2,000, followed by 2′ antibody 926-68073 (LI-COR) at a dilution of 1:20,000. Blots were scanned and quantified on a LI-COR Odyssey according to manufacturer's protocols.

Time-Lapse Fluorescence Microscopy Measurements

Life-extended HFFs and PML knockdown HFFs (a gift from Roger Everett) were passed onto a 96-well glass-bottom plate (Thermo Fisher Scientific) and grown to confluency to hold cells in the G0. Cells were synchronously infected on ice for 30 min at MOI = 1 (infection with mutant was done at room temperature). Live cells were imaged with a 20× oil objective on a spinning-disk confocal microscope (Olympus DSU) equipped with a 37°C, humidified, 5% CO_2 live-cell chamber. Image collection began when YFP signal was first detected and frames were captured every 10 min for 16–24 hr with an exposure time between 200 and 800 ms. Single-cell tracking and segmentation were performed with custom-written code in MatLab (Mathworks) as previously described (Weinberger et al., 2008). Homo-FRET imaging was performed as described (Weinberger and Shenk, 2007).

Mathematical Modeling to Estimate *H* from Time-Lapse Microscopy Data and Closed-Loop Analysis to Measure *H* from Flow Cytometry Data

Numerical simulations and fitting of an ODE model (Supplemental Information) were performed in Berkeley Madonna (www.berkeleymadonna.com).

Mathematica (Wolfram Research) was used for closed-loop analysis. Standard lentiviral cloning was used to create minimal MIE circuits (Dull et al., 1998). The minimal MIEP-IE2-GFP and MIEP-GFP circuits are driven by a full-length ~2.5 kb MIE promoter-enhancer (MIEP) that spans the sequence from the MIEP modulator at the 5′ edge to the junction of IE exons 1 and 2. The MIEP was PCR-cloned from AD169 into pLEIGW (a gift from Ihor Lemishka) in place of the EF1a promoter. This full-length MIEP drives an IE2-IRES-GFP or mCherry-IRES-GFP cassette. IE2 was cloned from pRSV-IE86 (a gift from Jay Nelson). ARPE-19 cells were infected and FACS sorted for GFP to create stably expressing cell lines (Figure S4). Cells were treated with TSA for 17 hr, and GFP expression was quantified by flow cytometry. Live cells were gated by forward-versus-side scattering on a FacsCalibur cytometer (BD Biosciences) and mean fluorescence intensity recorded. At least 20,000 live cells were recorded for each experiment, and data were analyzed in FlowJo (Treestar).

Replication Kinetics

Confluent MRC5 monolayers at ~5 × 10^4 cells per well were infected at indicated MOIs with 0.45 μm prefiltered virus inoculum stocks diluted in culture media. Inoculums were calculated based on plaque-assay titrations (Bolovan-Fritts and Wiedeman, 2001), shown as time point 0 in each figure. Inoculum was then removed and replaced with 1 ml of fresh medium. Infected wells were collected in triplicate at indicated time points and stored at −80°C. To measure replication, samples were thawed and prepared as a 10-fold serial-dilution series in culture medium analyzed by $TCID_{50}$, then converted to PFU/ml. Error ranges were calculated by standard deviation.

Minimal Synthetic Circuit Experiments

MIEP*Δcrs*-IE2-GFP was constructed by PCR cloning MIEP*Δcrs* from the CMV *Δcrs* IE2-YFP bacmid and inserted into MIEP-IE2-GFP. ARPE-19 cells were transduced with the MIEP-IE2-GFP and MIEP*Δcrs*-IE2-GFP vectors and FACS sorted for GFP. The transduced cell lines were allowed to recover for 24 hr before the percentage of GFP-expressing cells for each cell line was quantified. Live cells were gated by forward versus side scattering on a FacsCalibur cytometer. On the first day after recovery, 2,500 GFP events were recorded. Subsequently, at least 10,000 GFP events were recorded for each experiment and analyzed with FlowJo. For genomic PCR, genomic DNA was purified with a NucleoSpin Tissue kit (Clontech).

Immunofluoresence and Brdu-Labeled Virus Detection

Brdu-labeled virus was grown and detected by adapting a published method (Rosenke and Fortunato, 2004). Cells were grown on 16-well chamber slides (Lab-Tek) and infected with either CMV IE2-YFP or *Δcrs* IE2-YFP virus on ice and with 1% FCS media to synchronize infection. After 3 hr, cells were washed, fixed, and permeabilized (Rosenke and Fortunato, 2004). PML was

detected by a polyclonal PML rabbit antibody (Santa Cruz) at a 1:500 dilution, with secondary goat anti-rabbit Alexa 488 antibody (Invitrogen) at 1:500. After PML detection, the cells were stained with DAPI (Invitrogen) for 15 min before a second fixation with 3% formaldehyde. Brdu-labeled viral genomes were detected with a monoclonal rat Brdu antibody (Accurate Chemical Scientific Corp.) at 1:250, followed by secondary donkey anti-rat antibody conjugated with Alexa Fluor 568 (Invitrogen) at 1:500. Cells were mounted with ProLong Gold mounting media (Invitrogen) and a #1.5 coverslip (Nunc). Coverslips were imaged on a Zeiss Observer Z1 spinning-disk confocal microscope with a Plan-FLUAR 100×/1.45 oil objective. Colocalization analysis was performed in Slidebook 5.0 (Imaging Innovations).

SUPPLEMENTAL INFORMATION

Supplemental Information includes Extended Experimental Procedures, seven figures, one table, and four movies and can be found with this article online at http://dx.doi.org/10.1016/j.cell.2012.11.051.

ACKNOWLEDGMENTS

We are grateful to J. Ferrell, L. Fortunato, M. Elowitz, E. Mocarski, D. Spector, T. Hwa, A. Hoffmann, R. Tsien, J. Nelson, C. Lilley, M. Weitzman, and R. Everett for providing reagents, equipment, helpful discussion, and critical review of previous versions of this manuscript. We thank S. Thiberge and the Lewis-Sigler Imaging Core for invaluable technical expertise. M.W.T. and A.W. acknowledge support from NSF Graduate Research Fellowships. M.L.S. acknowledges support from the Center for Nanophase Materials Sciences, sponsored by the US Department of Energy. T.S. received support from the NIH (R01CA85786) and the NIH Center for Systems Biology at Princeton University (P50GM71508). This work was supported by NIH award K25GM083395 (L.S.W.). L.S.W. conceived and designed the study. M.W.T., C.B.-F., and L.S.W. designed and performed the experiments. M.W.T., C.B.F., R.D.D., M.L.S., T.S. and L.S.W. analyzed the data. A.W. and T.S. provided reagents. M.W.T., C.B.F., and L.S.W. wrote the paper.

Received: February 9, 2011
Revised: September 26, 2012
Accepted: November 27, 2012
Published: December 20, 2012

REFERENCES

Alon, U. (2007). An introduction to systems biology: design principles of biological circuits (Boca Raton, FL: Chapman & Hall/CRC).

Barrasa, M.I., Harel, N.Y., and Alwine, J.C. (2005). The phosphorylation status of the serine-rich region of the human cytomegalovirus 86-kilodalton major immediate-early protein IE2/IEP86 affects temporal viral gene expression. J. Virol. *79*, 1428–1437.

Black, H.S. (1999). Stabilized feed-back amplifiers (Reprinted from Electrical Engineering, vol 53, pg 114-120, 1934). Proc. IEEE *87*, 379–385.

Bolovan-Fritts, C., and Wiedeman, J.A. (2001). Human cytomegalovirus strain Toledo lacks a virus-encoded tropism factor required for infection of aortic endothelial cells. J. Infect. Dis. *184*, 1252–1261.

Bolovan-Fritts, C.A., Trout, R.N., and Spector, S.A. (2004). Human cytomegalovirus-specific CD4+-T-cell cytokine response induces fractalkine in endothelial cells. J. Virol. *78*, 13173–13181.

Bresnahan, W.A., and Shenk, T.E. (2000). UL82 virion protein activates expression of immediate early viral genes in human cytomegalovirus-infected cells. Proc. Natl. Acad. Sci. USA *97*, 14506–14511.

Cağatay, T., Turcotte, M., Elowitz, M.B., Garcia-Ojalvo, J., and Süel, G.M. (2009). Architecture-dependent noise discriminates functionally analogous differentiation circuits. Cell *139*, 512–522.

Carey, M., Peterson, C.L., and Smale, S.T. (2009). Transcriptional regulation in eukaryotes: concepts, strategies, and techniques, Second Edition (Cold Spring Harbor, N.Y.: Cold Spring Harbor Laboratory Press).

Cauwels, A., and Brouckaert, P. (2007). Survival of TNF toxicity: dependence on caspases and NO. Arch. Biochem. Biophys. *462*, 132–139.

Chen, J., Alberti, S., and Matthews, K.S. (1994). Wild-type operator binding and altered cooperativity for inducer binding of lac repressor dimer mutant R3. J. Biol. Chem. *269*, 12482–12487.

Chiou, C.J., Zong, J., Waheed, I., and Hayward, G.S. (1993). Identification and mapping of dimerization and DNA-binding domains in the C terminus of the IE2 regulatory protein of human cytomegalovirus. J. Virol. *67*, 6201–6214.

Choi, K.H., Basma, H., Singh, J., and Cheng, P.W. (2005). Activation of CMV promoter-controlled glycosyltransferase and beta -galactosidase glycogenes by butyrate, tricostatin A, and 5-aza-2′-deoxycytidine. Glycoconj. J. *22*, 63–69.

Cuevas-Bennett, C., and Shenk, T. (2008). Dynamic histone H3 acetylation and methylation at human cytomegalovirus promoters during replication in fibroblasts. J. Virol. *82*, 9525–9536.

Deshaies, R.J., and Ferrell, J.E., Jr. (2001). Multisite phosphorylation and the countdown to S phase. Cell *107*, 819–822.

Dull, T., Zufferey, R., Kelly, M., Mandel, R.J., Nguyen, M., Trono, D., and Naldini, L. (1998). A third-generation lentivirus vector with a conditional packaging system. J. Virol. *72*, 8463–8471.

Dwarakanath, R.S., Clark, C.L., McElroy, A.K., and Spector, D.H. (2001). The use of recombinant baculoviruses for sustained expression of human cytomegalovirus immediate early proteins in fibroblasts. Virology *284*, 297–307.

Everett, R.D., and Chelbi-Alix, M.K. (2007). PML and PML nuclear bodies: implications in antiviral defence. Biochimie *89*, 819–830.

Fan, S., Maguire, C.A., Ramirez, S.H., Bradel-Tretheway, B., Sapinoro, R., Sui, Z., Chakraborty-Sett, S., and Dewhurst, S. (2005). Valproic acid enhances gene expression from viral gene transfer vectors. J. Virol. Methods *125*, 23–33.

Flint, S.J.; American Society for Microbiology. (2009). Principles of virology, Third Edition (Washington, DC: ASM Press).

Garcia-Pino, A., Balasubramanian, S., Wyns, L., Gazit, E., De Greve, H., Magnuson, R.D., Charlier, D., van Nuland, N.A., and Loris, R. (2010). Allostery and intrinsic disorder mediate transcription regulation by conditional cooperativity. Cell *142*, 101–111.

Gardner, T.S., Cantor, C.R., and Collins, J.J. (2000). Construction of a genetic toggle switch in Escherichia coli. Nature *403*, 339–342.

Gautier, I., Tramier, M., Durieux, C., Coppey, J., Pansu, R.B., Nicolas, J.C., Kemnitz, K., and Coppey-Moisan, M. (2001). Homo-FRET microscopy in living cells to measure monomer-dimer transition of GFP-tagged proteins. Biophys. J. *80*, 3000–3008.

Gebert, S., Schmolke, S., Sorg, G., Flöss, S., Plachter, B., and Stamminger, T. (1997). The UL84 protein of human cytomegalovirus acts as a transdominant inhibitor of immediate-early-mediated transactivation that is able to prevent viral replication. J. Virol. *71*, 7048–7060.

Haase, A.T. (2010). Targeting early infection to prevent HIV-1 mucosal transmission. Nature *464*, 217–223.

Hofmann, H., Flöss, S., and Stamminger, T. (2000). Covalent modification of the transactivator protein IE2-p86 of human cytomegalovirus by conjugation to the ubiquitin-homologous proteins SUMO-1 and hSMT3b. J. Virol. *74*, 2510–2524.

Hooshangi, S., Thiberge, S., and Weiss, R. (2005). Ultrasensitivity and noise propagation in a synthetic transcriptional cascade. Proc. Natl. Acad. Sci. USA *102*, 3581–3586.

Hummel, M., and Abecassis, M.M. (2002). A model for reactivation of CMV from latency. J. Clin. Virol. *25*(*Suppl 2*), S123–S136.

Isomura, H., Stinski, M.F., Kudoh, A., Nakayama, S., Murata, T., Sato, Y., Iwahori, S., and Tsurumi, T. (2008). A cis element between the TATA Box and the transcription start site of the major immediate-early promoter of human cytomegalovirus determines efficiency of viral replication. J. Virol. *82*, 849–858.

Kobayashi, H., Kaern, M., Araki, M., Chung, K., Gardner, T.S., Cantor, C.R., and Collins, J.J. (2004). Programmable cells: interfacing natural and engineered gene networks. Proc. Natl. Acad. Sci. USA *101*, 8414–8419.

Ma, W., Trusina, A., El-Samad, H., Lim, W.A., and Tang, C. (2009). Defining network topologies that can achieve biochemical adaptation. Cell *138*, 760–773.

Macias, M.P., and Stinski, M.F. (1993). An in vitro system for human cytomegalovirus immediate early 2 protein (IE2)-mediated site-dependent repression of transcription and direct binding of IE2 to the major immediate early promoter. Proc. Natl. Acad. Sci. USA *90*, 707–711.

Mocarski, E.S., Shenk, T., and Pass, R.F. (2006). Cytomegaloviruses. In Fields' virology, D.M. Knipe, ed. (Philadelphia: Lippincott Williams & Wilkins), pp. 2708–2772.

Moorman, N.J., Cristea, I.M., Terhune, S.S., Rout, M.P., Chait, B.T., and Shenk, T. (2008). Human cytomegalovirus protein UL38 inhibits host cell stress responses by antagonizing the tuberous sclerosis protein complex. Cell Host Microbe *3*, 253–262.

Muzzey, D., Gómez-Uribe, C.A., Mettetal, J.T., and van Oudenaarden, A. (2009). A systems-level analysis of perfect adaptation in yeast osmoregulation. Cell *138*, 160–171.

Nevels, M., Brune, W., and Shenk, T. (2004). SUMOylation of the human cytomegalovirus 72-kilodalton IE1 protein facilitates expression of the 86-kilodalton IE2 protein and promotes viral replication. J. Virol. *78*, 7803–7812.

Nowak, M.A., and May, R.M. (2000). Virus dynamics: mathematical principles of immunology and virology (Oxford, New York: Oxford University Press).

Ozbudak, E.M., Thattai, M., Lim, H.N., Shraiman, B.I., and Van Oudenaarden, A. (2004). Multistability in the lactose utilization network of Escherichia coli. Nature *427*, 737–740.

Reddehase, M.J., and Lemmermann, N. (2006). Cytomegaloviruses: Molecular Biology and Immunology (Wymondham, UK: Caister Academic Press).

Rosenfeld, N., Elowitz, M.B., and Alon, U. (2002). Negative autoregulation speeds the response times of transcription networks. J. Mol. Biol. *323*, 785–793.

Rosenke, K., and Fortunato, E.A. (2004). Bromodeoxyuridine-labeled viral particles as a tool for visualization of the immediate-early events of human cytomegalovirus infection. J. Virol. *78*, 7818–7822.

Roth, J., Rummel, C., Barth, S.W., Gerstberger, R., and Hübschle, T. (2006). Molecular aspects of fever and hyperthermia. Neurol. Clin. *24*, 421–439, v.

Runnels, L.W., and Scarlata, S.F. (1995). Theory and application of fluorescence homotransfer to melittin oligomerization. Biophys. J. *69*, 1569–1583.

Sanders, R.L., Clark, C.L., Morello, C.S., and Spector, D.H. (2008). Development of cell lines that provide tightly controlled temporal translation of the human cytomegalovirus IE2 proteins for complementation and functional analyses of growth-impaired and nonviable IE2 mutant viruses. J. Virol. *82*, 7059–7077.

Savageau, M.A. (1976). Biochemical systems analysis: a study of function and design in molecular biology (Reading, Mass.: Addison-Wesley Pub. Co., Advanced Book Program).

Sourvinos, G., Tavalai, N., Berndt, A., Spandidos, D.A., and Stamminger, T. (2007). Recruitment of human cytomegalovirus immediate-early 2 protein onto parental viral genomes in association with ND10 in live-infected cells. J. Virol. *81*, 10123–10136.

Stinski, M.F., and Isomura, H. (2008). Role of the cytomegalovirus major immediate early enhancer in acute infection and reactivation from latency. Med. Microbiol. Immunol. (Berl.) *197*, 223–231.

Stinski, M.F., and Petrik, D.T. (2008). Functional roles of the human cytomegalovirus essential IE86 protein. Curr. Top. Microbiol. Immunol. *325*, 133–152.

Waheed, I., Chiou, C.J., Ahn, J.H., and Hayward, G.S. (1998). Binding of the human cytomegalovirus 80-kDa immediate-early protein (IE2) to minor groove A/T-rich sequences bounded by CG dinucleotides is regulated by protein oligomerization and phosphorylation. Virology *252*, 235–257.

Weinberger, L.S., and Shenk, T. (2007). An HIV feedback resistor: auto-regulatory circuit deactivator and noise buffer. PLoS Biol. *5*, e9.

Weinberger, L.S., Dar, R.D., and Simpson, M.L. (2008). Transient-mediated fate determination in a transcriptional circuit of HIV. Nat. Genet. *40*, 466–470.

Yu, D., Smith, G.A., Enquist, L.W., and Shenk, T. (2002). Construction of a self-excisable bacterial artificial chromosome containing the human cytomegalovirus genome and mutagenesis of the diploid TRL/IRL13 gene. J. Virol. *76*, 2316–2328.

Yu, D., Silva, M.C., and Shenk, T. (2003). Functional map of human cytomegalovirus AD169 defined by global mutational analysis. Proc. Natl. Acad. Sci. USA *100*, 12396–12401.

EXTENDED EXPERIMENTAL PROCEDURES

Theory

Derivation of a Model for Rate Acceleration: Approach I, Graphical Phase-Plane Argument

We consider one-dimensional ordinary differential equations of the general form:

$$\dot{x}(t) = f(\beta, x) - \delta x(t)$$

where *f* is an arbitrary function for "synthesis," which includes a basal "input" β that can be varied, δ is a fixed "decay" parameter, and *t* is time. To generate acceleration without amplification (i.e., rate acceleration), the function *f* must satisfy two criteria. First, the steady state of *x* must not vary significantly as β is increased—to limit any amplification—and second the rate of change of *x* (i.e., the right-hand side of the equation, which is the difference between *f(β,x)* and *δx(t)*), should be maximal for as long as possible—to generate the acceleration. A convenient way to examine these two criteria is to plot the synthesis function *f(β,x)* and the decay function *δx(t)* versus the value of *x*. The intersection of *f(β,x)* and *δx(t)* is the steady-state value—which we do not want to change significantly as β is increased—and the difference between *f(β,x)* and *δx(t)* is the rate—which we want to remain maximal for as long as possible.

There are two familiar classes of functions that have the potential to satisfy the criteria for rate acceleration: decaying exponentials and Hill functions:

$$f(\beta, x) = \beta e^{-x(t)} \text{ or } f(\beta, x) = \frac{\beta}{k + x(t)^H}$$

where *H* and *k* are fixed parameters and β is the basal synthesis rate. Importantly, the exponential and Hill functions are not the only functions with the potential to satisfy the two criteria for acceleration, but it is helpful to consider these two familiar functions because they are illustrative of the points that must be considered.

For the Hill function, we plot the synthesis function *f(β,x)* and the decay function *δx* versus the value of *x* for varying values of *H* (Figure S2). At low values of *H* (i.e., *H* = 0 or 1) the steady state of *x* (the intersection of each curve with the diagonal) ends up shifting to a significantly higher *x* value as β is increased. However, for higher values of *H* (*H* > 6) the steady state of *x* (intersection of each curve with the diagonal) remains almost unchanged as β is increased, and the rate (the difference between the curves and the diagonal) remains large across a broad range of *x* values.

We construct similar plots the exponential function $f(\beta,x) = \beta\, e^{-k-x(t)}$ for varying values of *k* (Figure S2). At higher values of *k* (i.e., *k* = 2) the change in the steady state of *x* appears to compress as β is increased (and below we explore this change in a more quantitative manner). However, the rate (the difference between the curves and the diagonal) does not appear to satisfy criterion 2 for acceleration because the difference between the synthesis and decay functions drops rather quickly for all values of *k*.

In summary, this graphical approach argues that a synthesis term that corresponds to the Hill functional form is able to satisfy both requirements for acceleration, whereas a synthesis functional form that employs exponentially decaying synthesis does not appear to satisfy the conditions for acceleration. In the next section we present a slightly more mathematical and quantitative approach to exploring, which functional forms can satisfy acceleration.

Derivation of a Model for Rate Acceleration: Approach II, Graphical-Analytic Argument

An alternate approach is to consider that acceleration requires the function *f* to satisfy the following two criteria:

Criterion 1 (no amplification):

$$\frac{\partial}{\partial \beta}\bar{x} \to 0$$

where $\bar{x}$ is the steady-state solution (i.e., satisfies $\dot{x}(t) = 0$). Criterion 1 states that the steady state value changes very little as "input" β is changed.

Criterion 2 (acceleration):

To achieve acceleration the slope of *x(t)* must be maximum at early times and must go to zero as the system approaches steady-state. So,

$$\frac{\partial}{\partial x}\dot{x}(t) \text{ must be maximal at } t = 0 \text{ (arbitrarily defined)} \Rightarrow \frac{\partial}{\partial x} f(\beta, x) \text{ must be maximal at } t = 0 \text{ (arbitrarily defined)}.$$

There are two familiar classes of functions with the potential to satisfy criterion 1, decaying exponentials and Hill functions:

$$f(\beta, x) = \beta e^{-x(t)} \text{ or } f(\beta, x) = \frac{\beta}{k + x(t)^H}$$

where *H* and *k* are fixed parameters and β is the basal synthesis rate.

Both the decaying exponential and the Hill function satisfy criterion 1. The decaying exponential function $f(x(t)) = \beta e^{-x(t)}$ gives a steady-state $\delta\overline{x} = \beta e^{-\overline{x}}$ solution of which is the Ω function (a.k.a. Product-Log function):

$$\overline{x} = \frac{ProductLog(\beta/\delta)}{\beta}$$

the slope of which (with respect to β) does indeed get exceedingly small (Figure S2). Similarly, the Hill function $f(\beta, x) = \beta/k + x(t)^H$ gives a steady state (for $k = 0$) of $\overline{x} = H - 1\sqrt{\beta/\delta}$ the slope of which (with respect to β) also becomes exceedingly small.

However, the decaying exponential $f(x(t)) = \beta e^{-x(t)}$ cannot satisfy criterion 2. Because $(\partial/\partial x) f(\beta, x) = (\partial/\partial x)\beta e^{-x} = -\beta e^{-x}$, which has a *minimum* at $t = 0$ (i.e., x = 0 because x*[0]* = 0) and actually has its maximum at $t = \infty$ (Figure S2). Importantly, the Hill function, $f(\beta, x) = \beta/k + x(t)^H$ does satisfy criterion 2:

$$\frac{\partial}{\partial x} f(\beta, x) = \frac{\partial}{\partial x}\left(\frac{\beta}{k + x^H}\right) = -\frac{\beta H x^{H-1}}{(k + x^H)^2},$$

which does have its maximum at $t = 0$ (i.e., x = 0 because *x[0]* = 0).

Although there are other potential functional forms that might satisfy criteria 1 & 2, the Hill function is familiar and provides well-known physical intuition pointing toward multimerization and self-cooperativity. For this reason, we focus on the models employing the Hill function.

Derivation of a Model for Rate Acceleration: Approach III, Gain-Bandwidth Argument

In electrical circuit theory, "loop-transmission" analysis is used extensively to determine stability, closed-loop response, transient response, and noise behavior of linear feedback systems and has been successfully applied to the analysis of genetic circuits (Austin et al., 2006; Cox et al., 2006; Simpson et al., 2003). The effect of negative feedback is to couple two system parameters—gain and bandwidth (response time in the time domain)—and thereby allow one to be traded for the other. To demonstrate, we consider the step response ($u(t)$ is the unit step function) of an amplifier circuit. The output, $O(t)$, is

$$O(t) = I\frac{A}{1 - T}\left(1 - e\frac{-(1 - T)t}{\tau}\right)$$

where A is the open loop gain of the circuit; I is the induction level, and we assumed a single time constant (τ). In most genetic circuits, τ would be determined by the protein half life and dilution rate (Austin et al., 2006; Simpson et al., 2003). The loop transmission, T, is the transfer function around the loop and may be thought of as a measure of the resistance of the feedback loop to variation (Simpson et al., 2003). For the circuit considered here $T = -A\beta$.

If T is a constant, the steady-state value and the rate of increase in the output are $O(t \to \infty) = I(A/1 - T)$ and $(dO(t)/dt) = (IA/\tau)e^{-(1-T)t/\tau}$. Some authors report that negative feedback speeds a circuit's response time, whereas others report the contrary result that negative feedback slows response. In fact, both views are correct. One may say that negative feedback speeds the response of the gene circuit because the circuit approaches steady state (i.e., $dO(t)/dt \to 0$) at a rate of 1-T faster than the nonfeedback circuit. Alternatively, one may say that negative feedback slows response as it decreases the absolute rate of increase $(dO_T = O(t > 0)/dt) > (dO_T < O(t > 0)/dt)$. This dichotomy arises because the decreased time to reach steady state is accompanied by a factor of 1-T reduction in the steady-state level (i.e., product of the gain and bandwidth (GBW product) of the circuit remains constant and the strength of the negative feedback controls the trade of one for the other).

Is it possible to achieve the speedier arrival at steady state without sacrificing the absolute rate of increase? The GBW product rule is in effect when T has a constant value over all time. However, an examination of the equation above shows that the GBW product relationship is established by repression that happens at two separate times: (1) repression of the rate of increase that occurs during the transient, and (2) repression of the steady-state level, which occurs at the end of the transient. A T that is variable such that it is small during the first of these periods and becomes larger during the second period provides both a speedier arrival to steady state and a fast rate of absolute increase during the transient. This variable T is accomplished in the CMV circuit with a high hill coefficient of the IE2 repression of the promoter, producing a T that increases significantly as IE2 population grows. That is, for the Hill expression:

$$\frac{dIE2}{dt} = \frac{I}{1 + (IE2/k_{IE2})^n} - \gamma IE2,$$

where γ represents the *IE2* decay/dilution rate, and k_{IE2} represents the IE2 population for 50% repression, there is almost no repression (feedback) until $IE2 \to k_{IE2}$ for high values of n. Furthermore, regardless of the induction level $IE2_{ss} \to k_{IE2}$, because repression increases sharply for $IE2 > k_{IE2}$. Until the circuit approaches steady state, negative feedback is essentially disabled, and the output grows at nearly the maximum rate. Near the steady-state level T abruptly increases, the rate of IE2 increase is quickly extinguished, and the steady-state level is quickly established.

This negative-feedback circuit motif has several distinguishing characteristics that may have biological significance. Foremost is that it produces an accelerator—larger induction levels speed the rise to the steady-state, but only weakly influence steady-state level. Additionally, this circuit topology has interesting noise behavior. Due to weak feedback strength, this circuit would be sensitive to noise during its transient rise to steady-state. Conversely, the strong feedback strength at the approach to and during maintenance of steady state would both reduce noise magnitude and shift the remaining noise to higher frequencies where it may have little biological effect (Austin et al., 2006; Simpson et al., 2003).

Minimal Circuit Models and Closed-Loop Analysis of Hill Coefficients

We used the analysis above to generate a standard two-dimensional model of gene expression (Alon, 2007; Kaern et al., 2005), and we arrive at the following model:

$$\frac{d}{dt}mRNA(t) = \frac{\beta}{k^H + protein(t)^H} - \varepsilon \cdot mRNA(t) \qquad \text{(Equation 1)}$$

$$\frac{d}{dt} = protein(t) = (1-f)\varepsilon \cdot mRNA(t) - \delta \cdot protein(t) \qquad \text{(Equation 2)}$$

This two-dimensional model describes the time evolution of *mRNA* and *protein* levels in the cell, and β represents the basal rate of promoter activity, k is a Michaelis-Menten type constant describing the threshold level below which autorepression does not act, H is the Hill coefficient describing the self-cooperativity in protein autorepression of the basal promoter activity, ε is a lumped rate constant describing the per-capita rate of *mRNA* export from the nucleus and translation into protein, f is the fraction of *mRNA* that is lost to *mRNA* decay prior to being translated into protein, and δ is the per-capita rate of protein decay (i.e., turnover). Because the *mRNA* species acts an exponential delay term (Alon, 2007; Murray, 2002; Savageau, 1976; Weinberger and Shenk, 2007), such systems of ordinary differential equations (ODEs) are commonly reduced and approximated by one-dimensional delay differential equations such as:

$$\frac{d}{dt}protein(t) = \frac{\beta}{k^H + protein(t-\tau)^H} - \delta \cdot protein(t) \qquad \text{(Equation 3)}$$

where τ acts as a fixed delay term. This simplified one-dimensional version of the model was used for the rate-balance analysis in Figure 2A and in the above sections (with $\tau = 0$ and $k = 1$). For simulations lacking feedback, H was set equal to zero. δ, the per-capita rate of protein decay (i.e., turnover), was set to 0.23 hr^{-1} the measured single-cell half-life of IE2 (Figure S6), which is in agreement with biochemical data (Dwarakanath et al., 2001).

For closed-loop Hill coefficient analysis, (Figure 2C) the steady-state for Equation 3 was numerically solved as β and H were varied, with a decay parameter value of δ = 0.23 hr^{-1} and a k value determined by fitting to the data obtained for the nonfeedback circuit MIEP-mCherry-IRES-GFP (Figure 2C).

Construction of the CMV MIE Circuit Model

The goal of generating a mathematical model of the CMV MIE circuit was only to fit the single-cell CMV IE2-YFP data from Figure 1D and the model is not intended to represent a comprehensive mathematical description of all known MIEP interactions or IE2-binding partners. Instead, our goal is utilitarian: to find the simplest model sufficient to fit the data in Figure 1E.

First, we expanded the minimal ODE model above to include IE1 protein, IE2 protein, and the MIE precursor mRNA. At the most fundamental level, the MIE locus is composed of the MIE promoter-enhancer (MIEP) driving two major alternative-splice variants that code for the 72-kDA IE1 protein and the 86-kDa IE2 protein, respectively (Stenberg, 1996). The MIEP is a relatively strong promoter (in transient transfection assays) and many cellular and viral activators including pp71, hDaxx, and NF-κB (Stinski and Isomura, 2008) are known to stimulate the MIEP. During CMV infection, the MIEP drives expression of a large "pre-mRNA" transcript that includes MIE exons 1-5 and is spliced into either the IE1 mRNA transcript (exons 2-4) or the IE2 transcript (exons 2, 3, and 5) (Stenberg, 1996). Once translated, the IE1 and IE2 proteins regulate other viral and cellular promoters but also autoregulate the MIEP (Meier and Stinski, 1996). IE2 downregulates the MIEP, whereas IE1 has a very weak positive regulatory effect on the MIEP (Fields et al., 2007), which is typically ignored.

For tractability, the quasi-steady-state assumption was applied to nuclear and cytoplasmic IE1 and IE2 mRNA levels, and a model utilizing three coupled ODEs describing MIE pre-mRNA, IE1 protein, and IE2 protein was developed.

$$\frac{d}{dt}MIE_{RNA} = \underbrace{\left(\beta}_{\text{basal act.}} + \underbrace{\frac{\alpha \cdot IE1^{H_1}}{k_1^{H_1} + IE1^{H_1}}}_{\text{IE1 activation}} \cdot \underbrace{\frac{1}{k_2^{H_2} + (\gamma \cdot IE2)^{H_2}}\right)}_{\text{IE2 repression}} - \underbrace{\delta \cdot MIE_{RNA}}_{\text{mRNA export/decay}} \qquad \text{(Equation 4)}$$

$$\frac{d}{dt}IE1 = \underbrace{f \cdot \lambda \cdot MIE_{RNA}}_{\text{IE1 translation rate}} - \underbrace{\delta_1 \cdot IE1}_{\text{IE1 protein decay}} \qquad \text{(Equation 5)}$$

$$\frac{d}{dt}IE2 = \underbrace{(1-f)\cdot\lambda\cdot MIE_{RNA}}_{\text{IE2 translation rate}} - \underbrace{\delta_2.IE2}_{\text{IE2 protein decay}} \qquad \text{(Equation 6)}$$

For tractability, the dimension of the left-hand side of each equation is only per hour (i.e., the state variables are dimensionless). Essentially, this model considers the following biochemical ''reactions'':

$$MIEP_{closed} \leftrightarrow MIEP_{open}$$

$$MIEP_{open} \xrightarrow{\beta} MIERNA_{precursor} + MIEP_{open}$$

$$MIERNA_{precurson} \xrightarrow{f} IE1RNA$$

$$MIERNA_{precurson} \xrightarrow{1-f} IE2RNA$$

$$IE1RNA \xrightarrow{\lambda} IE1$$

$$IE2RNA \xrightarrow{\lambda} IE2$$

$$H_1 \cdot IE1 \leftrightarrow IE1hmer$$

$$H_2 \cdot \gamma IE2 \leftrightarrow IE2hmer$$

$$IE1hmer + MIEP_{open} \leftrightarrow MIEP_{open\ 2}$$

$$MIEP_{open\ 2} \xrightarrow{\beta+\alpha} MIERNA_{precursor} + MIEP_{open} + IE1hmer$$

$$IE2hmer + MIEP_{open} \leftrightarrow MIEP_{repressed}$$

$$IE1RNA \xrightarrow{\delta} decay$$

$$IE2RNA \xrightarrow{\delta} decay$$

$$IE1 \xrightarrow{\delta_1} decay$$

$$IE2 \xrightarrow{\delta_2} decay$$

and this reaction-based model generates simulations that are qualitatively indistinguishable from the ODE model (data not shown). Thus, we concentrate on the ODE model. Equations 4, 5, and 6 describe MIE preprocessed mRNA transcripts, IE1 protein levels, and IE2 protein levels, respectively. β represents the MIEP basal promoter rate. The second term in Equation 4 accounts for IE1 autoactivation, or positive feedback, on the MIE promoter, and we assume that IE1 autoactivation on the MIE promoter saturates at some level (hence IE1 in both the numerator and the denominator to achieve an asymptotic function). Although IE1 transactivation is weak (Fields et al., 2007; Sambucetti et al., 1989), we included it in the model because we found it necessary for the model to fit the early-time concave-up curvature of the single-cell IE2-YFP trajectories during CMV IE2-YFP infection. α represents the rate of IE1 transactivation, and k_1 the Michaelis constant. Importantly, parameter-sensitivity studies (not shown) confirmed that the model is relatively insensitive to α and k_1 values and these parameter values can be varied over many orders of magnitude without altering the qualitative behavior of the system. The third term in Equation 4 represents IE2 autorepression on the MIEP with H being the Hill coefficient for IE2 that was varied for fitting to the data. k_2 represents the Michaelis constant, but sensitivity analysis (not shown) showed that model behavior is not significantly affected by altering this value (whereas altering k_2 does change the absolute value of the IE2 response-time, peak height, and steady-state, the relative differences for differing β or H do not change significantly with different k_2 values, thus, the Michaelis parameters do not significantly affect the calculation of H). γ represents the strength of IE2 autorepression. Although the values are not known, the IE2 repression rate and Michaelis constant should both be significantly smaller than those of IE1. This is because the strength of negative feedback is not strong enough to completely shut off the MIE promoter (Chiou et al., 1993; Macias and Stinski, 1993; Waheed et al., 1998) and IE2 directly influences the MIE promoter, unlike IE1 (Sambucetti et al., 1989). δ is a lumped parameter that represents the decay of MIE preprocessed mRNA transcripts and can include splicing of the preprocessed mRNA into alternative splice variants and nuclear export. Equation 5 and Equation 6 are essentially ''housekeeping equations'' that describe the production and turnover of IE1 and IE2, respectively. IE1 and IE2 are translated at a per capita rate λ and the fraction of MIE mRNA generating IE1 (f) versus IE2 (1-f) was calculated from published studies (Nevels et al., 2004). δ_1 represents the IE1 protein turnover rate and was calculated from previous studies (Stamminger et al., 1991) and single-cell experiments (data not shown) to be 0.032 hr^{-1}, whereas δ_2 represents the IE2 protein turnover rate and was calculated from previous studies (Stamminger et al., 1991) and single-cell analysis to be 0.23 hr^{-1} (Figure S6).

Upon increase of the MIE basal-expression rate, β, the rate of IE2 expression is markedly accelerated when λ is sufficiently small and $f > 1/2$. When $f > 2 \times (1 - f)$ or $f > 2/3$, there is a significant acceleration in the response-time of IE2. This observation agrees with experimental data in the literature that report IE1 being twice as abundant as IE2 (Nevels et al., 2004).

All parameters except the fraction of mRNA generating IE1 versus IE2 (*f*) and the IE1 and IE2 protein turnover rates (δ_1 and δ_2) were derived by performing nonlinear least-squares regression curve fitting with IE2-YFP single-cell trajectories for untreated cells and VPA-treated cells (Figure 1E). Best-fit curves were generated by varying values for model parameters while keeping δ_1 and δ_2 fixed. β was multiplied by 2 and 3 to fit IE2-YFP single-cell data under VPA 24 hr pretreatment and VPA 72 hr pretreatment, respectively, as the initial slopes of these IE2-YFP trajectories were 2- and 3-fold greater than trajectories from untreated cells.

To model the MIE circuit with the MIEP *Δcrs* promoter, the IE2 repression term in Equation 4 was set to zero.

Cloning of Recombinant Viruses

The CMV IE2-YFP virus was constructed in the CMV AD169 background (Bankier et al., 1991) by inserting EYFP (Clontech) to the 3′ end of IE2 exon 5 in the parent AD169 BAC as described (Moorman et al., 2008; Yu et al., 2002). The following IE2 targeting primers were used (sequences in capitals are the homology arms to IE2 sequence: 5′CTGAGCCTGGCCATCGAGGCAGCCATC CAGGACCTGAGGAACAAGTCTCAGgccggaagaagatggaaaaag3′ (forward); 5′ACGGGGAATCACTATGTACAAGAGTCCATGTCT CTCTTTCCAGTTTTTCACcgtcgtggaatgccttcg3′ (reverse).

The CMV GFP control virus (Yu et al., 2003) encodes an SV40 promoter-EGFP cassette. The CMV *Δcrs* IE2-YFP virus was constructed by BAC "recombineering" (Warming et al., 2005) of the CMV IE2-YFP virus as described (Cuevas-Bennett and Shenk, 2008). To propagate and purify virus, BAC DNA was electroporated (Yu et al., 2002) into MRC5 cells (American Type Culture Collection) with a GenePulser Xcell Electroporation System (Bio-Rad). Upon infection reaching 100% viral cytopathic effect or 100% GFP, the culture supernatant was collected and filtered with a 0.45 μm filter (Corning). For the CMV *Δcrs* IE2-YFP virus, low titers required concentration by ultracentrifugation: cells were disrupted by sonication to release virions, and supernatant was then filtered by a 0.45 μm filter and ultracentrifuged in a "sorbitol cushion" (20% D-sorbitol, 50 mM Tris-HCl, pH 7.2, 1 mM $MgCl_2$ in dH_2O) in an SW 41 Ti rotor (Beckman Coulter) at 25,000 rpm at 18°C. Viral stocks were titered by $TCID_{50}$ (Nevels et al., 2004). To verify the integrity of the CMV *Δcrs* IE2-YFP virus, a rescue virus, CMV *ΔcrsREVERT* IE2-YFP, was constructed by homologous recombination, whereby CMV *Δcrs* IE2-YFP BAC DNA (20 μg) and a ~2.5 kb wild-type MIEP DNA fragment (2.5 μg) were cotransfected by electroporation into 10^6 MRC5 cells, and subjected to two rounds of plaque purification.

Cell-Culture Conditions and Drug Perturbations

Cells were treated with a final concentration of 400 nM TSA (Sigma-Aldrich) resuspended in dimethylsulfoxide, for 20–24 hr, a final concentration of 10 ng/ml TNF-α (Sigma-Aldrich) resuspended in PBS, or a final concentration of 1 mM VPA (Calbiochem) for approximately 24 hr before imaging.

Time-Lapse Fluorescence Microscopy Measurements

Cells were passed onto a 35 mm glass-bottom dish (MatTek) or a 96-well glass-bottom plate (Thermo Fisher Scientific) and grown to confluency for several days to hold cells in the G0 phase. Cells were synchronously infected on ice at 4°C for 30 min or at room temperature for 30 min with virus at a MOI of 1. Live cells were imaged with a 20X oil objective on a spinning disk confocal microscope (Olympus DSU, Olympus America) equipped with a 37°C, humidified, 5% CO_2 live-cell chamber. Image collection began when YFP signal was first detected and frames were subsequently captured every 10 min for 16–24 hr with an exposure time between 200 and 800 ms. For IE2 half-life measurements, cycloheximide was added to cells 15 hr after infection, and cells were imaged every 10 min for 12 hr. Images were acquired with Slidebook 4.2 software (Imaging Innovations). Single-cell tracking and segmentation were performed with custom-written code in MatLab (Mathworks) as described (Weinberger et al., 2008). Code is available upon request. Homo-FRET imaging was performed as described (Weinberger and Shenk, 2007). FRAP imaging was performed on a FluoView 1000 confocal laser microscope (Olympus America). At 12 hr postinfection (h.p.i) (CMV IE2-YFP) or 24 hr postinfection (h.p.i.) (CMV *Δcrs* IE2-YFP), an initial snapshot was imaged and then a fixed pixel area within the nucleus (corresponding to ~1/4 to ~1/3 of the nucleus) was photobleached down to ~50% of its original intensity. The nuclei chosen for bleaching were roughly equivalent in size. An image was collected 30 s postbleach and then every minute for 25 min. Each image capture took 1,000 ms.

Analysis of Homo-FRET Data

The theoretical formula $r_n = r_1(1 \cdot (R_0/R)^6/1 + N(R_0/R)^6) + r_{et}((N-1)(R_0R)^6/1 + N(R_0R)^6)$ (obtained from (Runnels and Scarlata, 1995)) was solved for *N* (the number of IE2-YFP monomers bound together) for a range of possible r_n (the anisotropy value experimentally measured by homo-FRET) and *R* (the distance in Angstroms between any two IE2-YFP monomers in the homomultimer). The range of r_n represented in Figure 3B are the range of anisotropy values determined from our IE2-YFP homo-FRET experiments. r_{et} is defined as the anisotropy contribution from the 1st acceptor in the *N*-mer and assumed to be very small for large *N*-mers, making the 2nd term on the right hand side of the formula equal to 0. r_1 is the anisotropy value for a single IE2-YFP monomer randomly tumbling in space and is equal to 0.5, determined from our experimental homo-FRET results with CMV GFP virus. The calculated R_0, Förster distance, for an YFP-YFP interaction is 51.1 Angstroms (Patterson et al., 2000).

Western Blots

Sample preparation, protein transfer and blot preparation were handled as described earlier in quantitative western blot analysis methods (Bolovan-Fritts et al., 2004). For detection of bands, the blot was incubated with chemiluminescence substrate from the

Western Lightning ECL detection kit (NEN/Perkin-Elmer) according to the manufacturer's instructions. Protein bands were detected with a Typhoon PhosphoImager (GE Healthcare). The following antibodies and dilutions were used where indicated: primary mouse monoclonal anti-iE2 (clone 3A9) at 1:100 (Cuevas-Bennett and Shenk, 2008), a primary mouse monoclonal antibody against a shared epitope present in IE1 and IE2 at 1:100 (MAB810, Millipore), primary goat polyclonal anti-human actin at 1:2,000 (sc-1615, Santa Cruz Biotechology), secondary goat anti-mouse IgG conjugated to horse radish peroxidase (HRP) at 1:500 (sc-2005, Santa Cruz Biotechnology), and secondary donkey anti-goat IgG-HRP at 1:1,000 (sc-2020, Santa Cruz Biotechnology).

Immunofluorescence

Cells were grown on coverslips (VWR) in 24-well plate culture wells (CoStar) until ~60% confluency, then rinsed in cold PBS and fixed in 2% paraformaldehyde (Fisher Scientific) for 10 min at 4°C, blocked, and washed in PBS. IE2 protein was detected with the IE2-specific monoclonal antibody MAB8140 (Millipore) at a 1:200 dilution in blocking buffer for 1 hr at room temperature. A secondary donkey anti-mouse antibody conjugated to Texas Red (Santa Cruz Biotechnology) was used at a 1:500 dilution in blocking buffer, for 1 hr at room temperature in the dark. Samples were mounted in PBS and viewed with a 40× oil objective by confocal microscopy (Olympus DSU, Olympus America).

SUPPLEMENTAL REFERENCES

Austin, D.W., Allen, M.S., McCollum, J.M., Dar, R.D., Wilgus, J.R., Sayler, G.S., Samatova, N.F., Cox, C.D., and Simpson, M.L. (2006). Gene network shaping of inherent noise spectra. Nature *439*, 608–611.

Bankier, A.T., Beck, S., Bohni, R., Brown, C.M., Cerny, R., Chee, M.S., Hutchison, C.A., 3rd, Kouzarides, T., Martignetti, J.A., Preddie, E., et al. (1991). The DNA sequence of the human cytomegalovirus genome. DNA Seq. *2*, 1–12.

Cox, C.D., McCollum, J.M., Austin, D.W., Allen, M.S., Dar, R.D., and Simpson, M.L. (2006). Frequency domain analysis of noise in simple gene circuits. Chaos *16*, 026102.

Fields, B.N., Knipe, D.M., and Howley, P.M. (2007). Fields' virology, Fifth Edition (Philadelphia: Wolters Kluwer Health/Lippincott Williams & Wilkins).

Kaern, M., Elston, T.C., Blake, W.J., and Collins, J.J. (2005). Stochasticity in gene expression: from theories to phenotypes. Nat. Rev. Genet. *6*, 451–464.

Meier, J.L., and Stinski, M.F. (1996). Regulation of human cytomegalovirus immediate-early gene expression. Intervirology *39*, 331–342.

Murray, J.D. (2002). Mathematical biology, Third Edition (New York: Springer).

Patterson, G.H., Piston, D.W., and Barisas, B.G. (2000). Förster distances between green fluorescent protein pairs. Anal. Biochem. *284*, 438–440.

Sambucetti, L.C., Cherrington, J.M., Wilkinson, G.W., and Mocarski, E.S. (1989). NF-kappa B activation of the cytomegalovirus enhancer is mediated by a viral transactivator and by T cell stimulation. EMBO J. *8*, 4251–4258.

Simpson, M.L., Cox, C.D., and Sayler, G.S. (2003). Frequency domain analysis of noise in autoregulated gene circuits. Proc. Natl. Acad. Sci. USA *100*, 4551–4556.

Stamminger, T., Puchtler, E., and Fleckenstein, B. (1991). Discordant expression of the immediate-early 1 and 2 gene regions of human cytomegalovirus at early times after infection involves posttranscriptional processing events. J. Virol. *65*, 2273–2282.

Stenberg, R.M. (1996). The human cytomegalovirus major immediate-early gene. Intervirology *39*, 343–349.

Waheed, I., Chiou, C.J., Ahn, J.H., and Hayward, G.S. (1998). Binding of the human cytomegalovirus 80-kDa immediate-early protein (IE2) to minor groove A/T-rich sequences bounded by CG dinucleotides is regulated by protein oligomerization and phosphorylation. Virology *252*, 235–257.

Warming, S., Costantino, N., Court, D.L., Jenkins, N.A., and Copeland, N.G. (2005). Simple and highly efficient BAC recombineering using galK selection. Nucleic Acids Res. *33*, e36.

Yu, D., Smith, G.A., Enquist, L.W., and Shenk, T. (2002). Construction of a self-excisable bacterial artificial chromosome containing the human cytomegalovirus genome and mutagenesis of the diploid TRL/IRL13 gene. J. Virol. *76*, 2316–2328.

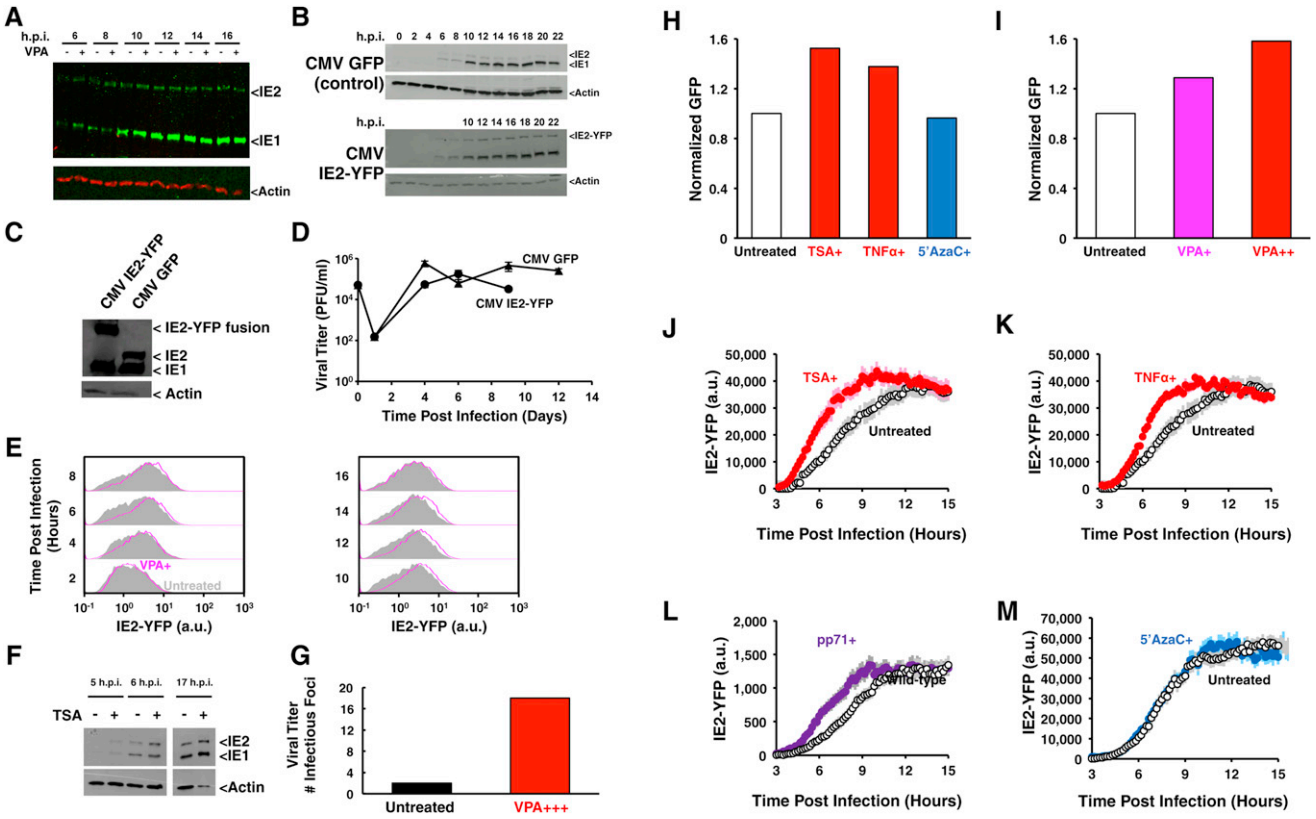

Figure S1. Acceleration by Time-Lapse Western Blot and Flow Cytometry, Comparison between IE2-YFP Virus and CMV GFP Control Virus, and Acceleration in a Clinical CMV Isolate, Related to Figure 1

(A) IE2-YFP protein levels, measured by western blot in CMV IE2-YFP virus infection, accumulate at the same rate as IE2-YFP fluorescence levels, measured by single-cell microscopy. Western blot time-course of IE2-YFP and IE1 levels after infection with CMV IE2-YFP virus (strain AD169) at an MOI = 1. VPA treatment accelerates both IE2 and IE1 protein expression, relative to an untreated control. Similar results were observed for TSA and TNF-α treatment (data not shown). These data further support that YFP fluorescence is a reliable reporter for IE2 protein levels.

(B) IE2 kinetics in CMV IE2-YFP virus are indistinguishable from IE2 kinetics in CMV GFP virus. Western blot time-course of IE2 levels after infection of cells with CMV IE2-YFP and CMV GFP viruses at MOI = 1.

(C) CMV IE2-YFP and CMV GFP viruses generate roughly equivalent levels of IE1 and IE2, respectively, upon infection.

(D) Fusion of YFP to IE2 does not significantly alter viral replication kinetics. Replication kinetics of CMV GFP virus (black triangles) and CMV IE2-YFP virus (black circles) at MOI = 1. Error bars (gray) represent ±1 SD.

(E) Flow cytometry measurements of IE2 kinetics support western blot and single-cell microscopy data. Histograms are shown every 2 hr from 2 hr postinfection (h.p.i.) to 16 hr.p.i for cells infected with CMV IE2-YFP virus in the presence (pink) and absence (gray) of VPA.

(F) Acceleration in the TB40-E clinical isolate of CMV. Western blot time-course of IE2 and IE1 levels after infection with TB40-E at MOI = 1.

(G) Number of infectious foci/1,000 cells after infection with TB40-E at MOI = 1 with or without 7 day VPA pretreatment.

(H) Live-cell flow cytometry GFP measurements of MIEP-GFP transduced cells demonstrating activation of the MIEP in presence of TSA (red), TNF-α (red), 5′azacytidine (blue), compared to no drug (white).

(I) Live-cell flow cytometry GFP measurements of MIEP-GFP transduced cells in presence of VPA at increasing incubation times (24 hr, pink; 72 hr, red) or absence of drug (white), demonstrating increasing activation of the MIEP.

(J) TSA activates the MIE promoter and accelerates IE2. Cells were infected in presence of TSA (red) or absence of drug (white). Error bars represent ±1 SE.

(K) TNF-α activates the MIE promoter and accelerates IE2. Cells were infected in presence of TNF-α (red) or absence of drug (white). Error bars represent ±1 SE.

(L) Viral pp71 activates the MIE promoter and accelerates IE2. An IE2-YFP virus carrying increased levels of the viral transactivator pp71 (purple), was generated and used to infect cells in parallel with IE2-YFP virus lacking extra pp71 (white). Error bars represent ±1 SE.

(M) 5′Azacytidine (a generalized DNA methylation inhibitor) treatment does not activate the MIE promoter and does not generate IE2 rate acceleration. Despite 5′azaC's ability to act as a generalized transcriptional activator, it clearly does not enhance transcriptional activity from the CMV MIEP in contrast to TSA and TNF-α. Cells infected in presence of 5′azaC (blue) show no acceleration in IE2 expression as compared to infection in absence of 5′azaC (white). Error bars represent ±1 SE.

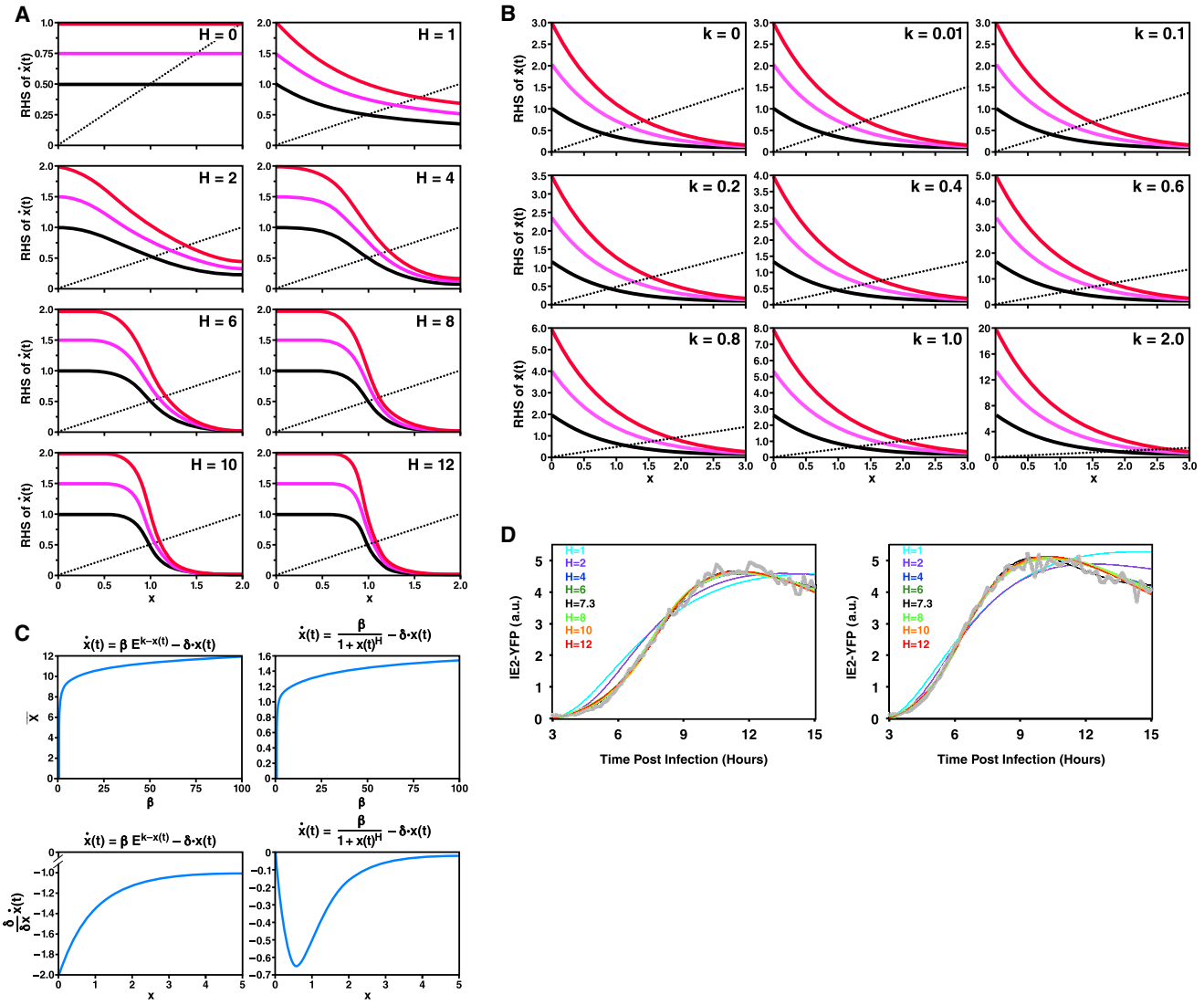

Figure S2. Models to Capture Acceleration without Amplification, Related to Figure 2

(A) Negative feedback with strong self-cooperativity generates acceleration without amplification. The expression of a gene product (x) over time is described by an ordinary differential equation (ODE): $\dot{x}(t) = f(\beta, x) - \delta x(t)$, where f is an arbitrary function for synthesis, which includes a basal input β that can be varied, δ is a fixed decay parameter, and t is time. The synthesis term is a Hill function: $f(\beta, x) = \beta / k^H + x(t)^H$ where H and k are fixed parameters. The plot shows a rate-balance analysis where the synthesis rate $f(\beta,x)$ and the decay rate $\delta \cdot x(t)$ are plotted versus the value of x for varying increasing of H in each subplot. Each plot shows solutions with δ = 0.5 (gray line) along with three values of β = 1 (black curve), β = 1.5 (pink curve), and β = 2 (red curve) where k = 1 for all plotted curves.

(B) Gene expression as a decaying exponential function does not generate acceleration. Here, the synthesis term uses a decaying exponential function: $f(\beta, x) = \beta e^{k - x(t)}$. Each subplot shows rate-balance analysis with δ = 0.5 (gray line) along with three values of β = 1 (black curve), β = 1.5 (pink curve), and β = 2 (red curve) for increasing k.

(C) The Hill function $f(\beta, x) = \beta / k^H + x(t)^H$ (where k = 1 for simplicity) satisfies two criteria necessary for acceleration without amplification, whereas the synthesis function described by the decaying exponential function $f(\beta, x) = \beta e^{k - x(t)}$ does not satisfy both criteria. Steady-state solutions of $\dot{x}(t) = f(\beta, x) - \delta x(t)$ show that both synthesis functions produce steady-state solutions ($\bar{x}$) that change very little as the basal input, β, increases. However, only the Hill function satisfies the criterion that the slope $(\partial / \partial x)\dot{x}(t)$ must be maximum at early times ($x(0)$ = 0) and must go to zero as the system approaches steady state.

(D) Sensitivity analysis of H for fits to single-cell data showing. Nonlinear least-squares regression of single-cell time-lapse microscopy data from Figure 1E (gray) to a mathematical model of the CMV MIE circuit (Table S1), showing best-fit curve of H = 7.3 (black) along with best-fit curves for H = 1 (cyan), H = 2 (purple), H = 4 (blue), H = 6 (dark green), H = 8 (light green), H = 10 (orange), and H = 12 (red). The best-fit curves were generated by allowing all models parameters to vary, while keeping H fixed. The sensitivity analysis was preformed for both the untreated control cells (left) and cells pretreated with VPA for 24 hr (right).

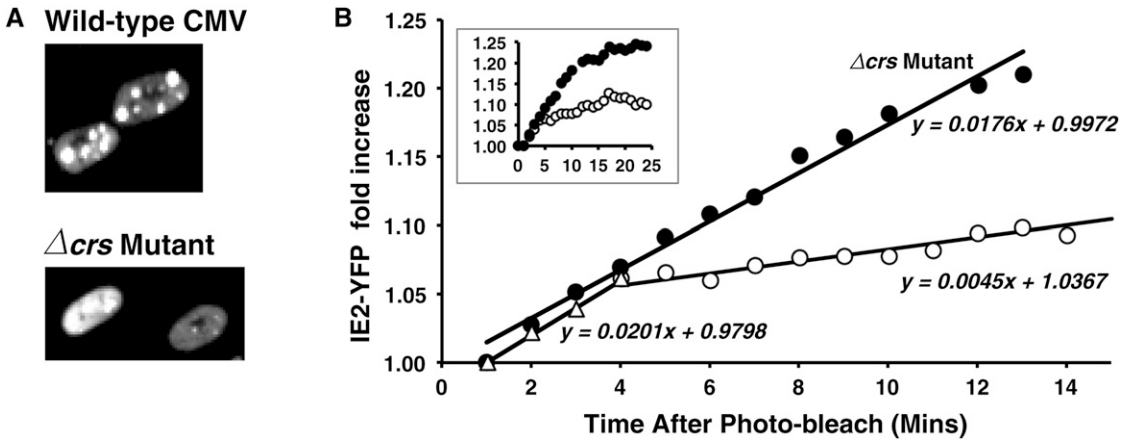

Figure S3. FRAP of IE2-YFP in Single Cells Reveals Two Effective Diffusion Coefficients for IE2, Related to Figure 3

(A) Live-cell fluorescence micrographs of cells infected with CMV IE2-YFP virus or CMV *Δcrs* IE2-YFP virus. CMV IE2-YFP virus exhibits the previously reported nuclear foci of IE2-YFP accumulation, but foci are largely absent from *Δcrs* IE2-YFP virus.

(B) Quantification of FRAP of live cells infected with CMV IE2-YFP or mutant *Δcrs* IE2-YFP virus (i.e., lacking the IE2 DNA-binding site). Cells were infected (at MOI = 1) with either virus, and when IE2 steady state was reached, 12 hpi or 24 hpi, respectively, a pixel-area corresponding to ~1/4 to 1/3 of the nucleus was photobleached down to ~50% its original intensity. All data were normalized by dividing by the initial intensity at the first capture time-point directly after photo-bleaching. Little recovery is observed during the first 30 s (data not shown), which is consistent with IE2′s numerous binding interactions with cellular proteins. During the first 4 min after bleaching, IE2-YFP in the bleached volume increases at the same rate for both parent and mutant. However, after 4 min, the parent exhibits a second slope that is ~4- to 5-fold lower (corresponding to a ~4- to 5-fold slower diffusion coefficient), whereas the mutant continues to increase in YFP accumulation in the bleached volume. The slower effective diffusion rate in the parent is consistent with a model where photo-bleached IE2 is stably bound to the DNA and excludes new IE2-YFP molecules from efficiently residing in the bleached volume. Inset: Full recovery trajectories showing that FRAP of *Δcrs* IE2-YFP viruses exhibits far greater recovery of absolute fluorescence as compared to FRAP to CMV IE2-YFP virus.

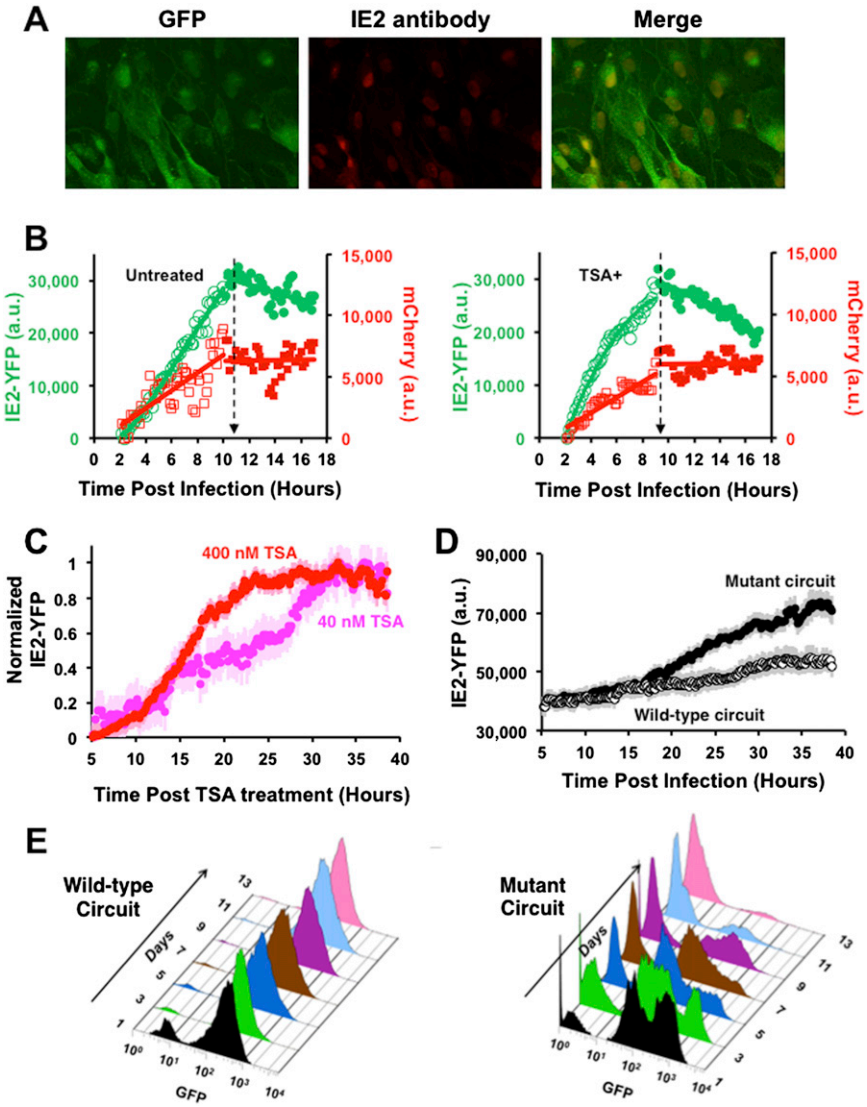

Figure S4. Confirmation of Stable IE2 Expression and MIE-Expression Kinetics from Integrated Lentiviral Vectors, Related to Figure 4

(A) Left: GFP fluorescence of ARPE-19 cells expressing the lentiviral vector MIEP-IE2-IRES-GFP. Center: Immunofluorescent staining of same cells with anti-iE2 antibody and Texas Red secondary antibody showing nuclear localization of IE2. Right: Overlay of GFP fluorescence and IE2 immunofluorescence.

(B) Human foreskin fibroblasts stably expressing a MIEP-mCherry leniviral vector were infected with CMV IE2-YFP virus (MOI = 1) in the presence (right) or absence (left) of TSA to generate two-color single-cell time-lapse microscopy trajectories (average of 20 cells) and track MIEP activity during CMV infection. The activity of the MIEP integrated within host genomic DNA (red) is highly correlated with CMV MIEP activity (green). The integrated MIEP exhibits negative autoregulation (plateau in mCherry levels) that is correlated with the maximum in IE2-YFP levels, and the integrated MIEP exhibits an accelerated rate of MIEP shutdown in the presence of TSA.

(C) Fluorescence quantification of single-cell GFP levels (20 cells) in cells expressing MIEP-IE2-IRES-GFP circuit in presence of 40 nM TSA (pink) or 400 nM TSA (red). Averages are shown in bold with ±1 SE shown in pink (400 nM TSA) or gray (40 nM TSA). IE2 expression accelerates with increasing levels of TSA.

(D) Fluorescence quantification of single-cell GFP levels (20 cells) in the negative-feedback MIEP-IE2-IRES-GFP circuit (white) and the feedback-knockout mutant MIEP*Δcrs*-IE2-IRES-GFP circuit (black) in presence of TSA. GFP levels are amplified in the mutant circuit compared to the wild-type circuit. Averages are shown in bold with ±1 SE shown gray.

(E) Live-cell flow cytometry time-courses of minimal circuits. The flow cytometry histograms of GFP fluorescence for wild-type circuit (left) and mutant circuit (right) used to construct Figure 4E trajectories. The percentage of GFP expressing cells for the wild-type circuit remains constant over time. The percentage of GFP expressing cells for the mutant circuit decreases over time. The relatively high percentage of cells displaying low GFP fluorescence on day 1 in the wild-type circuit may be due to sorting-induced cytotoxicity and the short recovery time for cells after FACS sorting.

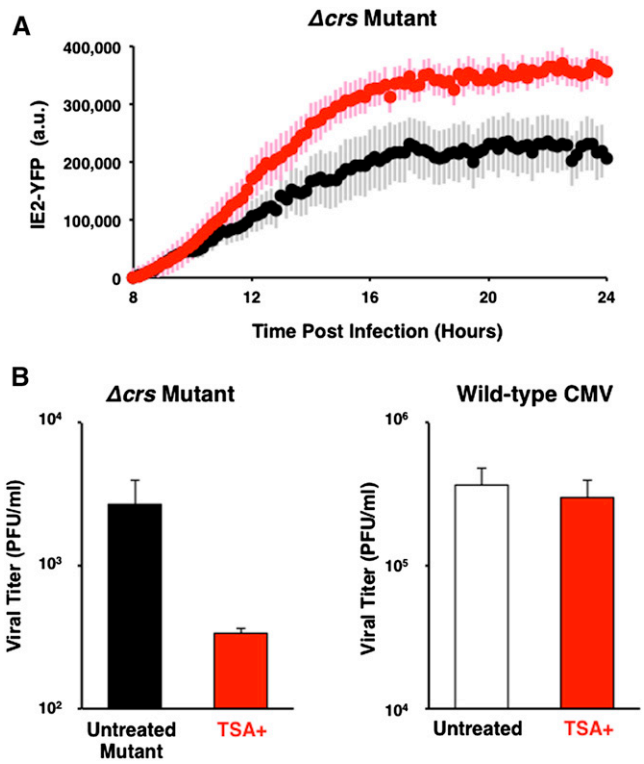

Figure S5. Eliminating IE2 Negative Feedback Abrogates Rate Acceleration and Generates Level Amplification, Producing a Significant Fitness Cost for the Virus, Related to Figure 5

(A) Time-lapse microscopy results of cells undergoing infection with CMV *Δcrs* IE2-YFP mutant virus in presence of TSA (red) or absence of TSA (black). Trajectories are averages of 20 cells (bold) together with ±1 SE (lighter background).

(B) Raw viral titers (measured by plaque forming units, PFU/ml) of cells infected with CMV *Δcrs* mutant virus in presence (red) and absence (black) of TSA. Averages are shown with ±1 SD in bold gray for day 9 postinfection. Decreased viral titer after TSA treatment is not due to TSA toxicity to cells at day 9 because cells treated with TSA and subsequently infected with CMV IE2-YFP virus do not exhibit a significant a drop in titer, compared to untreated cells on day 10 (see C).

(C) Raw viral titers (measured by plaque forming units, PFU/ml) of cells infected with CMV IE2-YFP virus at an MOI of 0.2 in presence (red) and absence (white) of TSA. Averages are shown with ±1 SD in bold gray for day 10 postinfection.

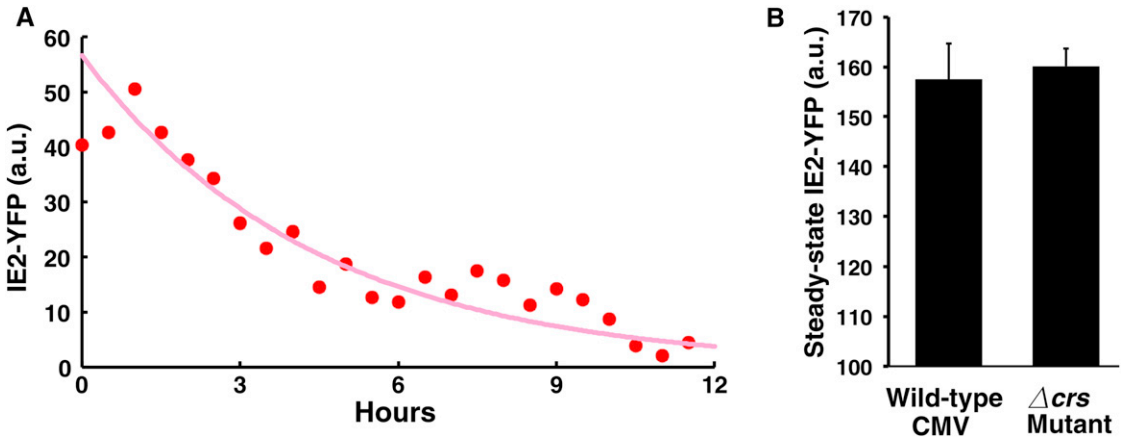

Figure S6. Ablating IE2 Negative Feedback Does Not Increase IE2-YFP Levels in the Mutant Virus Compared to the Wild-Type IE2-YFP in the Viral Setting; Changes in IE2 Decay Are Unlikely to Explain Lack of IE2 Increase because IE2 Already Exhibits a Very Short Protein Lifetime, Related to Figures 6

(A) IE2 half-life calculated from single-cell microscopy is 0.23 hr^{-1}. IE2-YFP single-cell kinetics were measured after cycloheximide addition at 15 hr postinfection. An average of 20 cells is shown (red), and the data were fit to a decaying exponential (pink). The exponential decay argues against nonlinear decay models to explain the IE2 acceleration phenotype.

(B) Flow cytometry measurement of steady-state IE2-YFP levels of CMV IE2-YFP and CMV *Δcrs* IE2-YFP viruses measured agree with single-cell microscopy measurements. Steady-state was measured at 15 hr.p.i for CMV IE2-YFP and 24 hr.p.i. for *Δcrs* IE2-YFP virus. Error bars in black are ±1 SD.

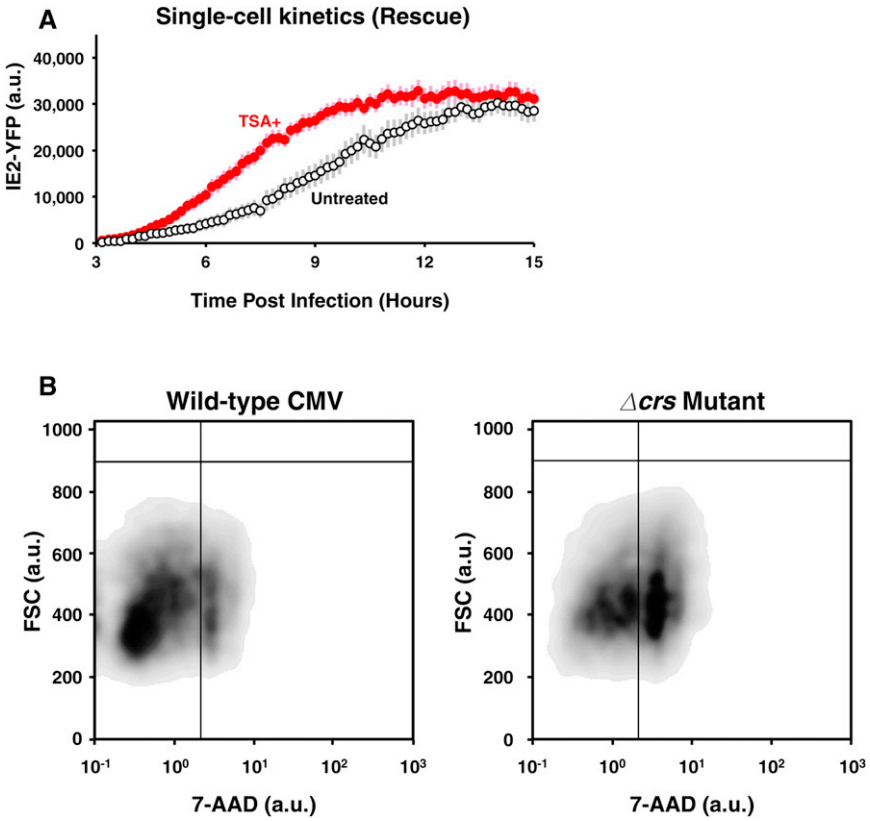

Figure S7. Rescue of the *Δcrs* Mutation to Wild-Type Sequence Results in Recovery of Rate Acceleration; Accelerator Circuitry Provides a Fitness Advantage over Amplifier Circuitry by Decreasing Virus-Induced Cell Death, Related to Figures 7

(A) Single-cell fluorescence microscopy trajectories of rescue virus IE2-YFP levels in presence (red) or absence (white) of TSA after an MOI = 1 infection. Averages of 20 cells shown in bold with ±1 SE shown in pink (TSA) or gray (no drug).

(B) Flow cytometry density plot of cells infected for 7 days with CMV IE2-YFP or CMV *Δcrs* mutant virus (at equal MOIs) and stained with 7-AAD to detect live and dead populations. Approximately half of the CMV *Δcrs* mutant population are positive for 7-AAD signal (right, bottom right quadrant) and are nonviable, whereas only 23% of the CMV IE2-YFP population (left, bottom right quadrant) are nonviable.